Ion/Ion Reactions in Primary Structure Interrogation of Intact Proteins by Mass Spectrometry

Elizabeth Milda Duselis

Indianapolis, Indiana

Bachelor of Science in Biochemistry, Purdue University, 2012

A Dissertation Presented to the Graduate Faculty of the University of Virginia in Candidacy for the Degree of Doctor of Philosophy

Department of Chemistry

University of Virginia

December, 2019

Abstract

This dissertation describes method development for intact protein characterization by mass spectrometry with ion/ion reactions. In this first project, novel methodology of sequential ion/ion reactions, electron transfer dissociation (ETD) followed by ion/ion proton transfer, is used on intact hemoglobin subunits in clinical samples to identify single amino acid substitutions. In this study, 22 variants were definitively identified, including a previously unreported hemoglobin variant now known as Hemoglobin Charlottesville.

In the second portion of the dissertation, ion/ion reaction kinetics play a pivotal role. A novel method for investigating the physics of ion motion during an ion/ion reaction is presented. By applying a supplemental alternating current electric potential during the ion/ion reaction, resonant ions are indirectly evaluated through arrested reaction rates. This method uncovered alterations to ions' fundamental secular frequencies in a quadrupole ion trap due to simultaneous confinement of both ion polarities. This knowledge builds the basis for development of parallel ion parking during ETD, an analytical method in which first-generation ETD fragments are resonantly excited. The arrested reaction rate of these ions lead to their preservation. The resulting sequence coverage of standard proteins 8.6 kDa

ubiquitin, 17 kDa apomyoglobin, 20 kDa histone H1, and 21 kDa Protein G are 96%, 88%, 73%, and 80% respectively. The high incidence of complementary fragment ion pairs (93%, 78%, 85%, and 85% respectively) are promising for the future of intact protein interrogation.

Acknowledgements

Don. Oh, Donald. That gem of a human being and class act of a scientist. Five years ago, Don (very quietly) explained to me in his office for the first time about gas phase ion/ion chemistries and that Graham Cooks is one of his favorite scientists. The latter was quite the recruiting hook. In the Hunt Lab, I was given freedom to pursue my interests, make mistakes, and grow as a scientist at my own rate. Thank you, Don, for being a wonderful role model, both personally and professionally. And thank you for signing this dissertation despite all the grief I've given you.

Jeff Shabanowitz is my favorite little ray of pragmatic sunshine. He has instilled in me the obsessive need to question how everything works and the firm belief that anything can be fixed. He taught me how to think analytically, a gift that extends into all aspects of my life. Thank you, Jeff, for not kicking me out of lab after all the stuff I've broken.

Dina Bai might be the best of humankind. As a scientist, she is brightly optimistic every problem has a solution. As a person, she is brightly optimistic every problem has a solution. Her unending support, encouragement, patience, and understanding come without judgment. Thank you, Dina, for teaching me to be a less pessimistic scientist and a better friend.

I'm greatly indebted to my collaborators. I am appreciative of the opportunity to have worked with Dave Herold and his post doc Jane Yang at UC San Diego, as well as their unending patience with me. Most of this dissertation would not have been possible without the guidance of John EP

Syka and Chris Mullen of Thermo Fisher Scientific. Thank you, John and Chris, for patiently interpreting my babble on the weekly conference calls and giving your time to my research. I learned a lot directly from your explanations, but you also taught me to think critically about the underlying physics of my experiments and be a better analytical scientist. I'm continually amazed by your creativity when suggesting experiments. John, thank you especially for being a wonderful mentor to me. While your scientific guidance has been absolutely invaluable, it is also your dedication to grad students and honest science that I will always strive to emulate.

Thank you to Professors Kevin Lehmann, Andreas Gahlmann, Ken Hsu, and David Brautigan for serving on my defense committee. I am appreciative of your willingness to spend time and energy reviewing this thesis and participating at my defense.

Being a part of the Hunt Lab was an experience I'll always treasure, especially for the people I've met. Ben Barnhill had the misfortune of sharing desk space with me my first three question-filled years. He inspired me with his simple and accessible science explanations to focus on improving my communication skills. Thank you, Rob and Jenna, for being my friends; you guys (together and individually) always make me smile. Keira Mahoney is a treasure in so many ways I can't even begin to describe, and I'm proud to be her friend.

Stephanie Miller Lehmann got me through my first summer and second (and third through fifth) year of grad school. She expanded numerous

horizons for me with her friendship. Stephanie, you is kind, you is smart, and you is stuck with me now. Joel, you're ok.

I've had the good fortune to stumble upon great friends while in grad school. Maura Belanger has been with me through everything, since TA training before our first semester. Maura, you absurdly loyal Hufflepuff, thank you for dealing with my hangriness. Thank you, Andi Davis and Eric Hunt, for your friendship; it has meant the world to me. Katy Wilson, words cannot express my gratitude for you in my life, so I need you to just pretend this sentence is the hug of a lifetime.

More so than any other point in my life, I have realized and appreciated over the past five years how much I am loved and supported by my family, especially my parents. My brother John reminds me of that every month, whether I want to hear it or not. My sisters Rosemary, Marian, and Tania have been invaluable support especially. My favorite brothers, Mark and Peter, have saved my sanity multiple times, mostly by fixing my car.

Table of Contents

List of Figures

Chapter 1

Chapter 2

Chapter 3

List of Tables

Chapter 2

Abbreviations

μ	micro ($1x10^{-6}$)
AGC	automated gain control
A, Ala	alanine
AC	alternating current
C, Cys	cysteine
C18	octadecylsilane
CAD	collision activated dissociation
CID	collisional induced dissociation
D, Asp	aspartic acid
Da	Dalton
DC	direct current
DNA	deoxyribonucleic acid
E, Glu	glutamic acid

ESI	electrospray ionization
ETD	electron transfer dissociation
ETnoD	electron transfer reaction with no dissociation
F, Phe	phenylalanine
FWHM	full width at half maximum
FT	Fourier transform, or high resolution
g	grams
G, Gly	glycine
Hb	hemoglobin
H, His	histidine
HPLC	high pressure liquid chromatography
I, Ile	isoleucine
i.d.	inner diameter

IIPT	ion/ion proton transfer
IT, ITMS	ion trap or low resolution mass analysis
k	kilo ($1x10^3$)
K, Lys	lysine
L	liter
L, Leu	leucine
LC	liquid chromatography
LIT	linear ion trap
m	milli ($1x10^{-3}$)
M	molar
M, Met	methionine
min	minute
mol	mole

ms	milliseconds
MS	mass spectrometry
MS^1	full mass spectrum, scan of ions available without manipulation
MS^2, MS/MS	tandem mass spectrum, scan of ions after isolation and manipulation (i.e. fragmentation)
MS^3, MS/MS/MS	tandem mass spectrum, scan of ions after ion produced in MS/MS fragmentation are further fragmented
Mw	molecular weight
m/z	mass-to-charge ratio
n	nano ($1x10^{-9}$)
N, Asn	asparagine
NaCl	sodium chloride

NL	non-linear, way of normalizing ion counts
o.d.	outer diameter
OT	Orbitrap
p	pico ($1x10^{-12}$)
P, Pro	proline
PIP	parallel ion parking
ppm	parts per million
PTM	post translational modification
Q, Gln	glutamine
r	resolution
R, Arg	arginine
rcf	relative centrifugal force
RF	radio frequency

S, Ser	serine
S/N	signal-to-noise ratio
T, Thr	threonine
TIC	total ion current
V	volt
V, Val	valine
w/w	weight-to-weight
W, Trp	tryptophan
Y, Tyr	tyrosine

Chapter 1

1. Introduction to the Dissertation

1.1 Overview

This dissertation is comprised of three projects, unified in their objective through use of ion/ion reactions and mass spectrometry to characterize the primary structure of intact proteins. The second chapter employs novel methods in ion/ion reactions to characterize clinically relevant proteins, the third chapter characterizes the physics of ion motion during the ion/ion reaction, and the fourth chapter describes the innovation of a new method to improve sequence coverage of intact proteins through manipulation of ion/ion reaction kinetics.

In the second chapter, human clinical samples are analyzed by mass spectrometry to identify hemoglobin variants that contain single amino acid mutations. Single amino acid substitutions can adversely affect hemoglobin's intended function of transporting oxygen from the tissue to the lungs. Current clinical evaluations are multi-tiered and prone to misidentification. Thus, a robust, sensitive, and accurate analytical method such as mass spectrometry would ease clinical analysis of hemoglobin variants. Additionally,

a previously unreported hemoglobin variant was discovered, now known as Hemoglobin Charlottesville.

In Chapter 3, ion motion during the ion/ion reaction in a quadrupolar ion trap is explored. The effects on ion motion of simultaneous confinement of anions and cations in the ion trap has not been previously characterized. Herein is presented a novel method to indirectly determine the exact frequency of motion of an ion in the quadrupolar field during the ion/ion reaction. Deviations from an ion's fundamental secular frequency were unexpectedly observed and influencing factors were characterized.

In Chapter 4, a method to enhance sequence coverage of intact proteins through manipulation of ion/ion reaction kinetics is presented. Selective inhibition of the ion/ion reaction rate of specific ions is demonstrated to preserve sequence-informative fragments and promote efficient fragmentation of the precursor protein. This chapter describes endeavors to refine the method and make the technology user-friendly.

The focus of the first chapter of this dissertation will be to cover the basic principles of proteins, mass spectrometry, and ion/ion reactions which will be the foundation of the following chapters.

Chapter 1

1.2 Proteins

A protein is a chain of linked amino acids. An amino acid is composed of a central carbon atom (α carbon) linked to an amino group, a carboxyl group, a hydrogen, and a unique functional side group. The chain is held together by peptide (or amide) bonds between the carboxylic group of one amino acid and the amine group of the next, so that the chain has a free amine at one end (N-terminus) and free carboxyl at the opposite end (C-terminus), as seen in Figure 1.1. If the side chains are removed from consideration, the protein then consists of a "backbone" of regularly repeating subunits of peptide linkages.

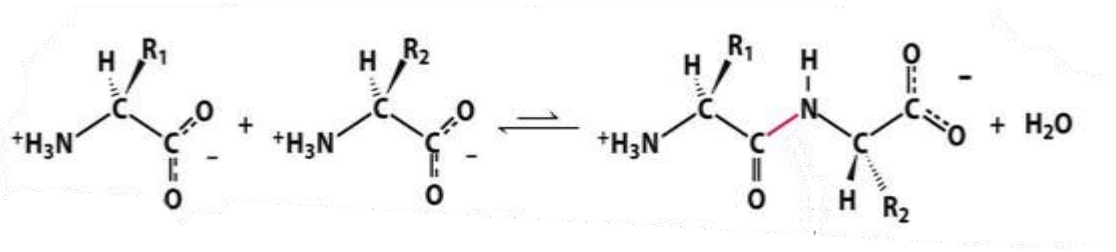

Figure 1.1. The linking of two amino acids is accompanied by the loss of a water molecule. Highlighted in pink is the peptide bond.

There are 20 common amino acids; each of these amino acids have a 3-letter abbreviation and one letter code (Figure 1.2.) Protein sequences are

usually written N-terminus to C-terminus, left to right, using the one letter codes. Each amino acid in a protein is a "residue."

The protein's amino acid sequence is also called its primary structure. The interactions of the unique side groups as determined by their position in the primary structure determines the protein's 3-dimensional structure. Since protein function is directly dependent on the 3-dimensional structure, knowing protein primary structure is essential to understanding a protein's function.

1.2.1 Primary structure interrogation by mass spectrometry

In recent decades, the complexity of the human proteome has been increasingly realized; current estimates place nearly 1 million proteins in its composition (1). This diversity has led to the recognition that protein variation plays a pivotal role in the complexity afforded by biological systems. Distinct protein forms modulate different biological processes; therefore, determining a protein's primary structures and modifications to that structure is essential to fully understanding the biological processes.

Mass spectrometers, instruments that measure a gas phase ion's mass-

to-charge ratio (m/z,) have become the principal tool for protein analyses due to the high sensitivity, high mass accuracy, and ease of analysis. A spectrum of all ions entering a mass spectrometer at a given time is referred to as an MS or MS^1 scan. Protein primary structure interrogation proceeds by a technique known as tandem MS (MS/MS or MS^2), in which a selected protein precursor ion from the MS scan is isolated and broken down into fragment ions; it is the fragment ions that then undergo m/z evaluation. Characteristic mass differences between the fragment ions correspond to the 20 amino acids, allowing for reconstruction of the primary structure. Identification of 5-6 sequential amino acids is typically enough to uniquely identify the parent protein through proteome database searching (2). Less commonly, MS/MS/MS or MS^3 interrogation can be employed, in which a selected ion from the MS/MS fragmentation is isolated and further fragmented (2).

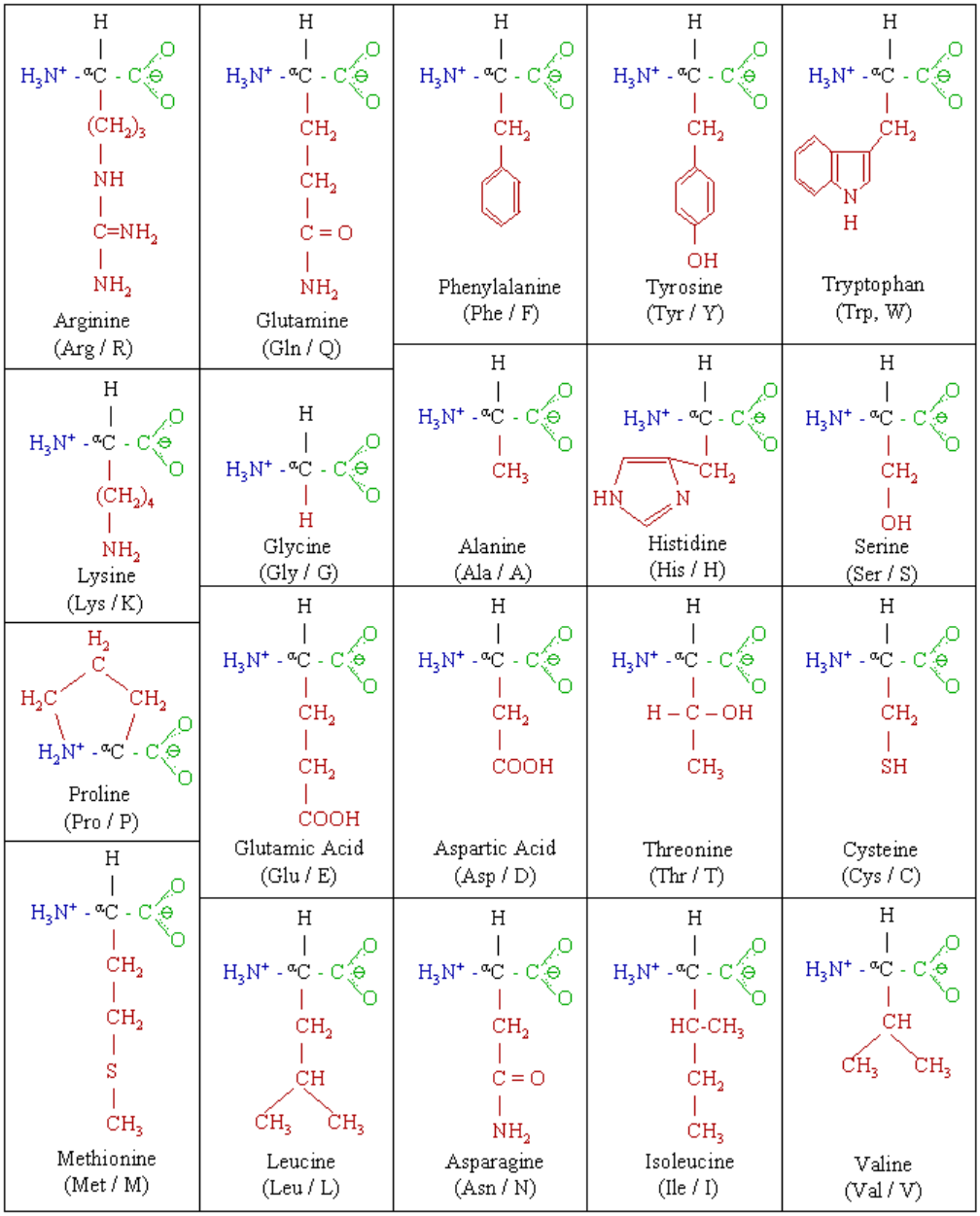

Figure 1.2. The 20 common amino acids of proteins. Amino groups are blue, carboxyl groups are green, the C_α is black, and side chains are red.

Chapter 1

To determine the primary structure, MS/MS interrogation needs to break the precursor ion systematically along the peptide backbone. A single peptide backbone cleavage will produce two complementary fragment ions, which are categorized by the position of the cleavage and which protein terminus the fragment contains (2). For example, as seen in Figure 1.3, breaking the N-C_α bond produces a c-type ion that contains the protein's N-terminus and z-type ion that contains the protein's C-terminus.

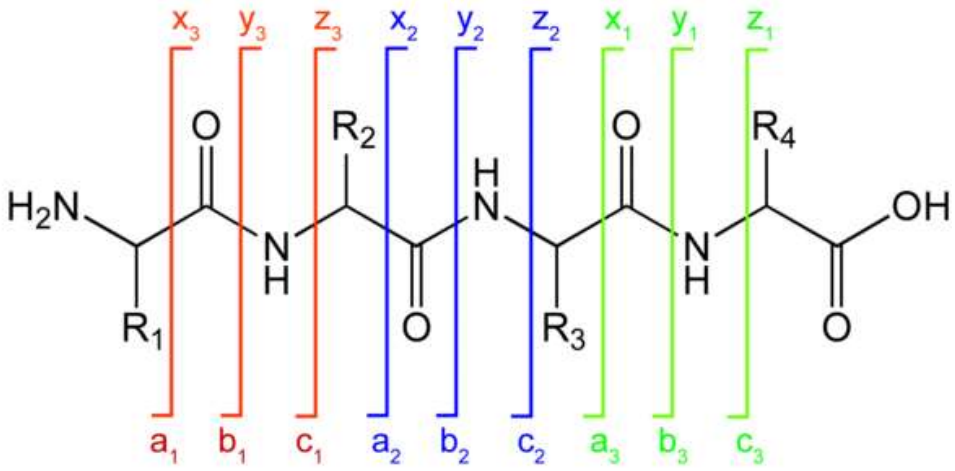

Figure 1.3. Protein fragment ion nomenclature. Protein fragment ion series are classified by where on the protein backbone the cleavage occurs and which terminus of the protein the ion contains. For a-, b-, and c-type ions, the ion contains the protein's N-terminus. The protein's C-terminus is included with x-, y-, and z-type ions.

1.3 Overview of mass spectrometry experiment

A mass spectrometer operates at low pressures, which allows for ion manipulation through electric potentials on various electrodes in the mass spectrometer. Every mass spectrometer has an ionization source, some configuration of electrodes, and a mass analyzer. Relevant characteristics of protein ions and details of primary structure interrogation by MS are summarized briefly below.

All of the MS experiments referenced in this dissertation were performed on a ThermoFisher Scientific™ Orbitrap™ Elite mass spectrometer (the Elite) (3). The Elite contains several distinct sets of devices: an ionization source, an ion optics system for transmission of ions throughout the instrument, a Dual Pressure Linear Ion Trap, and a high resolution Orbitrap mass analyzer. A full diagram of the Elite is shown in Figure 1.4.

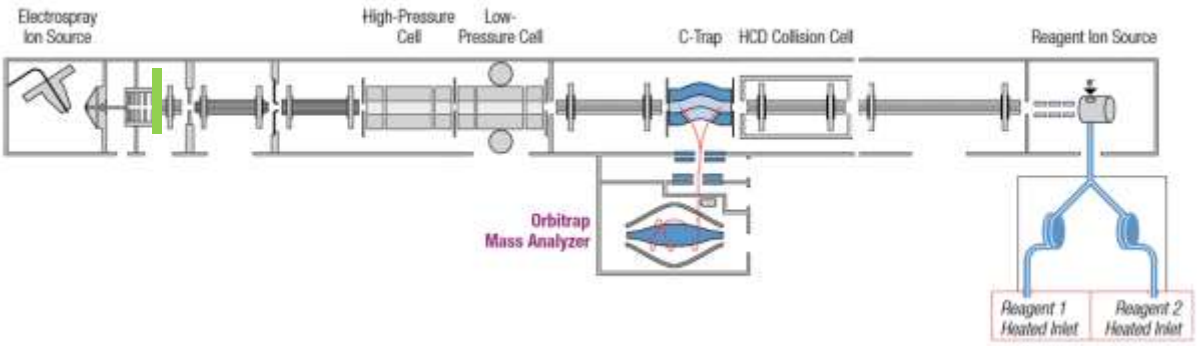

Figure 1.4. Diagram of Orbitrap™ Elite. Precursor ions are introduced at the electrospray ion source and are stored in the high pressure cell. Both IIPT and ETD reagent anions are ionized via a custom glow discharge source positioned just after the S-lens (green). For high resolution mass analysis, ions are transferred to the C-trap and subsequently injected into the Orbitrap mass analyzer. Figure adapted from (6).

1.3.1 Ionization and bio-ion characteristics

As mass spectrometers can only manipulate and detect gaseous ions, the first stage of MS analysis is electrospray ionization (ESI) of the protein analyte and introduction into the mass spectrometer. In this process, the protein is sprayed through a small diameter needle in an acidic aqueous/organic solution (typically water/acetonitrile or water/methanol.) A high voltage is applied to this needle to produce an aerosol from a Taylor cone. These droplets have positive charges due to protons provided by the acidic solution. Droplet evaporation leads to the formation of smaller droplets from which ions are desorbed (4).

Chapter 1

Characteristically, ESI produces $[M + zH]^{z+}$ gaseous cations from proteins in acidic solutions, where M is the molecule, z is the number of final charges, and H denotes a proton. The protein can acquire a variable number of protons, creating a distribution of final charge states. The signal for a single analyte is split into multiple m/z peaks. The number of protons acquired depends on many factors, such as ionization voltage, protein gas phase basicity, solution composition, flow rate, protein conformation in solution, and inlet capillary temperature. Typically, the larger the protein, the more charges a protein will acquire during ESI. A small peptide, like the 10mer angiotensin II, typically acquires 2 or 3 protons to form either $[M+2H]^{+2}$ or $[M+3H]^{+3}$. A larger protein, like the 153 residue apomyoglobin, forms $[M+26H]^{+26}$–$[M+40H]^{+40}$ from the 26-40 protons imparted by ESI.

1.3.2 Ion motion and ion optics

Once in the gas phase, ion manipulation is solely determined by the ions' m/z identity. In the mass spectrometer's vacuum environment (<1e-5 torr), the absence of a dielectric medium makes ions extremely responsive to Coulombic attraction and repulsion to electric potentials on electrodes; e.g.,

cations are strongly attracted to the negatively charged electrodes and repelled when the electrode has positively charged character. In this way, ion motion is manipulated through alternating current (AC) and direct current (DC) potentials on the various optics of the mass spectrometer. How fast ion motion responds to these electric potentials depends on the ion's mass (m) and charge (z).

After ionization, various devices (or configuration of electrodes, such as quadrupoles, multipoles, and lenses) are used to guide the ions through the mass spectrometer. Axially, ion motion is guided by a static potential gradient between successive devices. For protein cations, each successive device has an increasingly negative DC potential to pull the cation through to the next device. Radially, the ions are confined by radio frequency AC potentials applied to the multipoles that continually attract and repel the ions such that the ions never touch an electrode surface.

1.3.3 Dual Pressure Linear Ion Trap system: High Pressure Cell and Low Pressure Cell

The Elite has two linear ion traps (LITs), a high pressure cell and low pressure cell. The electrode configurations have identical dimensions, but

high pressure cell's pressure is 7e-5 torr while the low pressure cell is 1e-5 torr. The variant pressures in these cells are optimized for function. Higher pressures are more optimal for ion collisional cooling, ion storage, and fragmentation. Collisions with a buffer gas limit mass spectral performance by reducing resolution and contributing to mass shifts that limit mass accuracy; the low pressure cell is better suited for mass analysis (5).

Ions lose axial kinetic energy by collisions with the helium bath gas as they enter the high pressure LIT. The collisional cooling helps to stably trap more ions than would be with electric fields alone. Once trapped in the high pressure cell of the LIT, ions can be stored or manipulated for ion/ion reactions; unwanted ions can be ejected from the LIT. The high pressure cell is especially functional for collisional activated dissociation (CAD), a process by which ions are resonantly kinetically excited so that the collisions with the bath gas imparts enough vibrational energy to fragment the protein precursor. Ions can also be transferred to the low pressure cell for low resolution mass analysis or to the C-trap for high resolution mass analysis (5, 6). The LIT is discussed in greater detail in 1.4.

1.3.4 Orbitrap Mass Analyzer

For high resolution mass analysis, ions are transferred from the high pressure LIT to the AC-only C-trap, another ion trap designed to aid ion injection into the Orbitrap, as seen in Figure 1.5. Axial motion of the ions is reduced by gentle collisions with nitrogen in the C-trap. Once stably confined in the C-trap, the electric potentials on the electrodes leading to the Orbitrap are lowered, injecting ions into the Orbitrap. Radially, the electric fields of the Orbitrap and rotational inertia force the ions to adopt a circular orbit around the central electrode. Axially, the ions oscillate axially in m/z-dependent frequencies:

$$\omega_{Orbitrap} = \sqrt{\left(\frac{z}{m}\right)k} \qquad (1.1)$$

where $\omega_{Orbitrap}$ is the angular frequency of the ions oscillating in the axial direction and k is the force constant of the quadratic restoring potential related to the geometry of the electrodes. As the ions oscillate, a differential amplifier detects a current induced by the ions on the split outer electrode.

The image current is Fourier transformed into ion frequencies and subsequently into a mass spectrum (7).

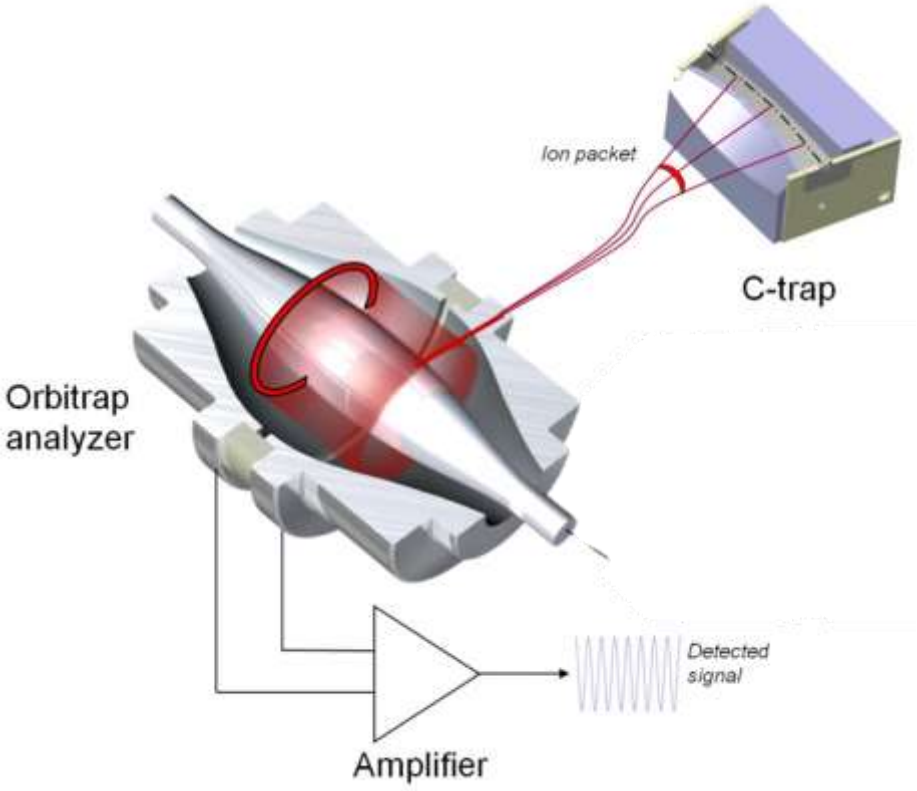

Figure 1.5. Orbitrap™ mass analysis. Figure adapted from (7).

1.4 The Linear Ion Trap

Since much of the work presented in this dissertation involves phenomena associated with the LIT, a detailed description of the device is provided.

1.4.1 Configuration

The LIT was developed by Schwartz, Senko, and Syka in 2002 as a multipurpose device that can perform ion trapping, isolation, ion/ion reactions, CAD, and low resolution mass analysis. It is composed of 3 electrically isolated segments, each with 4 parallel rods with hyperbolic profiles as depicted in Figure 1.6. The front and back sections are 12 mm long, and the center section is 37 mm long (8).

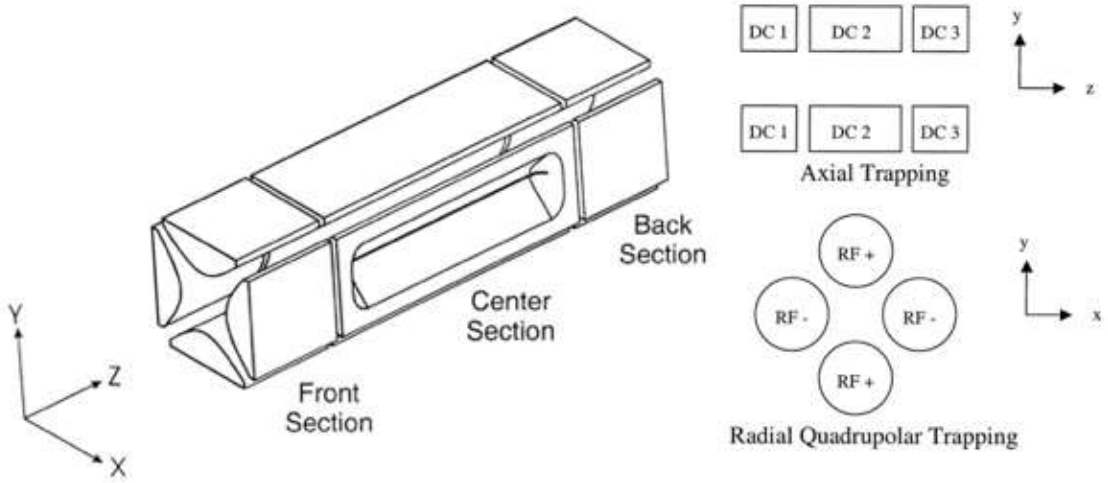

Figure 1.6. The quadrupole linear ion trap. Figure adapted from (8).

Radiofrequency AC potentials ("RF") 180 degrees out of phase are applied to adjacent rods for radial confinements of the ions as shown in Figure 1.6 (referred herein as "main RF" or "trapping RF"). Each of the three sections can have a different DC offset, allowing for axial confinement of ions in the center section in a potential well (8–10).

On the x-rods of the center section are 30 mm long slits, outside of which are positioned conversion dynodes and electron multiplier systems for low resolution mass analysis by resonance ejection (10). Aside from the main trapping RF, an additional AC potential can be superposed onto the x-rods for resonant excitation of the ions (11).

1.4.2 Quadrupole field: Mathieu parameters and ion secular frequency

Ion motion in an ion trap is explained in depth in March and Todd's Quadrupole Ion Trap Mass Spectrometry; a summary from this source is presented below (12).

The hyperbolic profile of the 4 electrodes in the LIT creates a "quadrupolar field" in the x-y plane, an electric field in which the potential at a point varies quadratically with distance from the center of the LIT:

$$\emptyset_{x,y} = \frac{\emptyset_0}{2r_0^2}(x^2 - y^2) \quad (1.2)$$

where x and y are the dimensions of the quadrupole field, Φ is the potential at a given point within the field, and r_0 is half the distance between opposite electrodes.

Ion motion in the quadrupolar field can be described by the Mathieu equation. The Mathieu equation is a second order differential formulated in the 19th century to describe vibration interactions in a stretched animal skin. Solutions to the Mathieu equation are used to describe conditions under which a particle experiences a changing but cyclical force. Thus, the Mathieu equation can be applied to ion motion in the quadrupolar field generated

principally by oscillating AC potentials to correlate physically meaningful quantities (like mass and charge) to ion stability and frequency of oscillation in the trap.

The Mathieu equation takes the form:

$$\frac{d^2u}{d\xi^2} + (a_u - 2q_u \cos 2\xi)u = 0 \qquad (1.3)$$

where u is displacement, ξ is a time-dependent parameter defined as ξ =Ωt/2, Ω is the angular frequency of the main trapping RF, and a_u and q_u are dimensionless Mathieu parameters. Trajectory and stability can be correlated to an ion's Mathieu parameters. In the LIT, an ion's Mathieu parameters are:

$$a_x = -a_y = \frac{8zU}{mr_0^2\Omega^2} \qquad (1.4)$$

$$q_x = -q_y = \frac{-4zV}{mr_0^2\Omega^2} \qquad (1.5)$$

where z is the ion's charge, U is the DC potential applied to the rods in a quadrupole manner, V is the zero-to-peak voltage of the trapping RF potential, and m is the mass of the ion. Note that each parameter is inversely dependent on the ion's m/z ratio.

Chapter 1

An ion's Mathieu parameters a_u and q_u (where u is quadrupole dimension x or y) can be used to describe stable ion trajectories in the LIT. Regions of stable trajectories are shown in the Mathieu stability diagram in Figure 1.7. Any ion defined by an (a_u,q_u) parameters in the shaded region of Figure 1.7 will be successfully trapped in the LIT; other ions will be ejected or will collide with the electrodes. Typically, LITs are operated without DC potentials, so that a_u=0 and all ions are on the q_u axis. In these circumstances, ions with $0.050 \lesssim q_u < 0.908$ are stably trapped. Because q_u is inversely proportional to an ion's m/z, ions will be distributed on the q_u axis as a reciprocal of their m/z values. Higher m/z ions will have lower q_u values, and low m/z ions adopt higher q_u values.

The quadrupolar field of the LIT oscillates an ion in a m/z-dependent frequency in the x- and y- dimensions, which is referred to as the ion's secular frequency. Mathieu parameters can be used to describe an ion's secular frequency. When a_u=0, an ion's secular frequency, ω, in dimension u:

$$\omega_{u,0} = \frac{q_u \Omega}{2\sqrt{2}} . \quad (1.6)$$

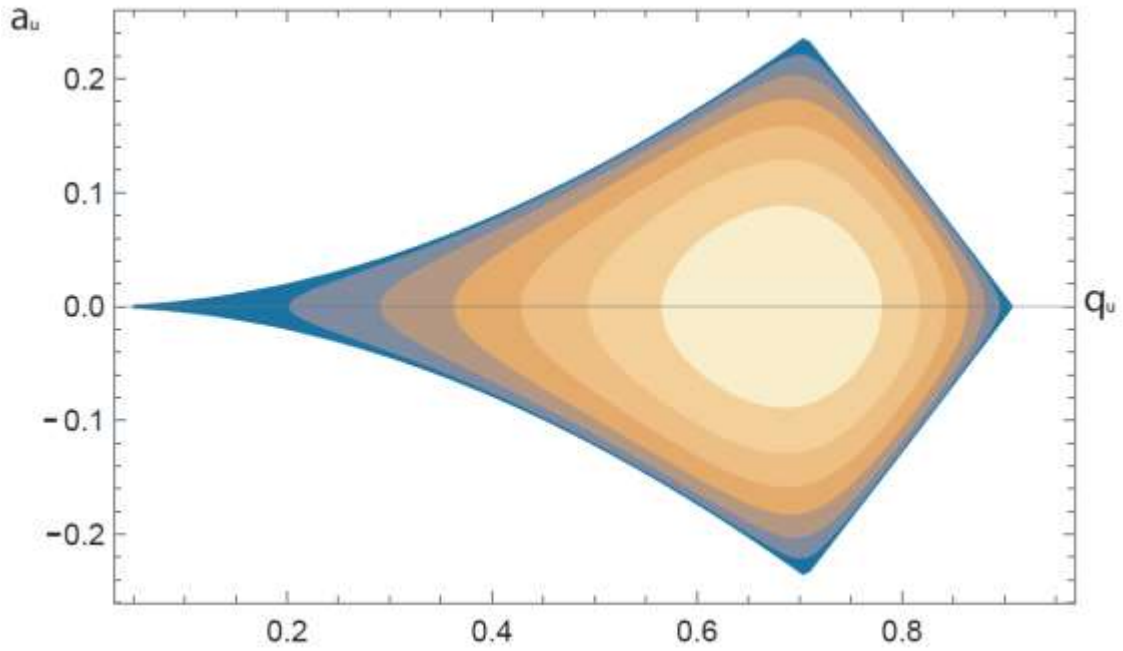

Figure 1.7. Mathieu stability diagram for ions in an LIT. Ions defined by (a_u, q_u) parameters in the shaded (blue and gold) region are stably confined in the LIT.

An ion's secular frequency and m/z have an inverse relationship. Lower m/z ions have a higher Mathieu q_u and higher secular frequency of oscillation in the LIT; higher m/z ions have a lower Mathieu q_u and lower secular frequency of oscillation in the LIT. This relationship is also correlated to higher mass dispersion at low secular frequencies/q_u but lower mass dispersion at high secular frequencies/q_u.

1.4.3 Resonant Excitation in a Quadrupolar Electric Field

The fortunate relationship between secular frequency and m/z (Equation 1.6) allows resonances to be used for mass-selective manipulation of ion populations in the LIT, such as ion ejection and kinetic excitation.

Resonant excitation is similar to pushing a child on a swing. The child has a frequency of motion. Exerting a force in a time-dependent manner that matches the child's frequency of motion will increase the amplitude of the child's motion. Similarly, when a supplementary AC potential is superposed across the trapping RF of the x-rods, the ions with secular frequencies matching the auxiliary AC frequency increase in kinetic energy. Those resonantly kinetically excited ions have increased radial amplitude of oscillation and average velocity (11, 13).

Resonant kinetic excitation has several purposes in MS analyses. In the low pressure LIT, ions are mass-selectively ejected from the trap through a slit in the electrodes into a conversion dynode; correlating the resonant frequency of ejection with an electron multiplier response yields a low-resolution mass spectrum (8). As mentioned in 1.3.3, the MS/MS technique of CAD uses

resonant excitation of an ion to increase the energy of collisions with the bath gas, so that the ion will fragment (9, 12).

It is possible to excite many ions at once. Instead of superposing a single supplemental AC potential to the x-rods, many AC potentials are applied in the form of a waveform. Each ion with a secular frequency matching a frequency component of the waveform is resonantly kinetically excited. In this way, it is possible to selectively resonantly kinetically excite a swath of ions with varying m/z values simultaneously (11).

1.4.4 Automatic Gain Control

Ions have their own electric field from their elementary charge(s). For small numbers of ions, this field is negligible compared to the electric field created by the main RF on the LIT's electrodes. However, the field strength grows with the number of ions being confined. Therefore, all ion trap instruments have a limit to the number of elementary charges that can be stored before the charges distort the electric field created by the trapping electrodes. Once these space charge limits are reached, the ability to excite or isolate the ions is compromised. Additionally, mass spectra resolution and

accuracy are severely reduced (9). Therefore, a process known as automatic gain control (AGC) is employed to control the number of ions entering the ion trap. Prior to every scan, all ions entering the mass spectrometer at that time accumulate in the low pressure LIT for a very short, fixed injection time. These ions are ejected through the slits in the electrodes into a set of electron multipliers for current detection. This allows for estimation of the flux of ion current (in charges per second) into the instrument at that time. Using the ion current detected in this short pre-scan, the instrument adjusts the ion accumulation time for the next analytical scan to reach the ideal number of charges or "target."

1.5 Ion/ion reactions

The LIT can be used as reaction vessel for ion/ion reactions, in which cations and anions are simultaneously stored. Here, we restrict our discussion to ion/ion reactions with protein precursor cations and singly charged reagent anions. These reactions proceed in one of three ways: an electron is transferred from the anion to the precursor prompting dissociation (electron transfer dissociation), a proton is transferred from the precursor to the anion

(ion/ion proton transfer), or some combination of the preceding two reactions occurs. The mechanism of the reaction depends on the chemical identity of the reagent (14).

1.5.1 Electron Transfer Dissociation

In 2004, Hunt and colleagues introduced electron transfer dissociation (ETD), an ion/ion reaction in which a radical reagent anion transfers an electron to a polypeptide precursor cation during simultaneous confinement in the LIT (15). The resulting odd-electron species undergoes fragmentation pathways driven by radical chemistry, cleaving the N-C_α bond to generate c- and z·-type ions, as detailed in Figure 1.8.

It is important to note that not every electron transfer reaction forms two observable fragment ions. The product from electron transfer with no dissociation (ETnoD) reactions is the intact precursor reduced by one charge, since the electron transfer neutralizes a charge on the cation. There are many reasons for ETnoD. Fragmentation N-terminal to a proline residue will break the N-C_α bond but the precursor is kept intact through the side chain ring

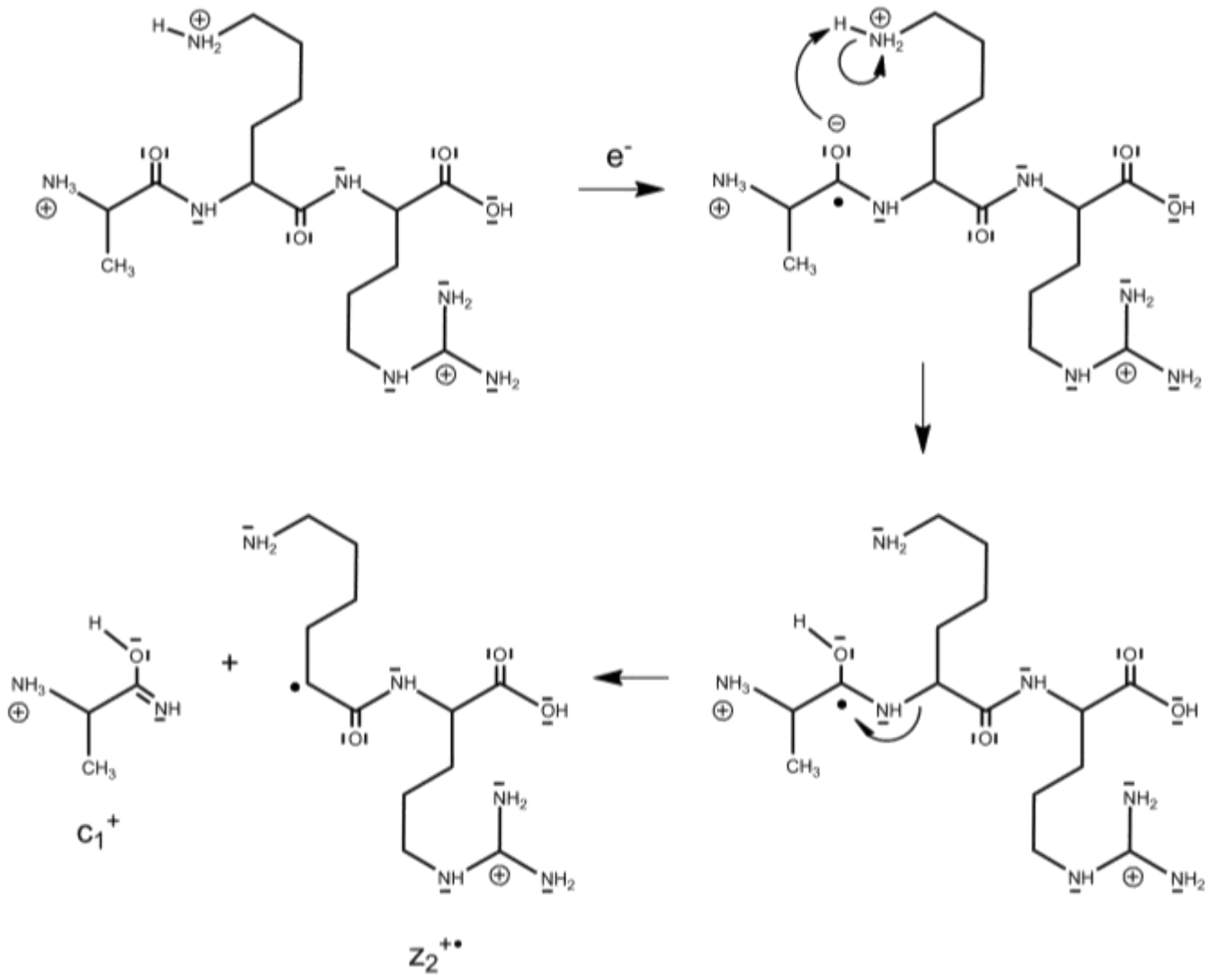

Figure 1.8. ETD mechanism

structure (15). Hydrogen bonding and electrostatic interactions within the precursor can keep the two fragment ions associated in the gas phase (16).

Radical sites formed by electron transfer near a histidine can stabilize through isomerization of the imidazole side chain (17). Electron transfer to the precursor can simply result in H· ejection, still reducing the charge of the precursor without observable dissociation (18). A proton could also be transferred to the anion from the precursor, although this reaction can be minimized through careful selection of reagent anion (14, 19).

1.5.2 Ion/ion Proton Transfer

In ion/ion proton transfer (IIPT) reactions, the reagent anion abstracts a proton from the precursor cation. This reduces the charge of the precursor by one unit without fragmentation (14, 20).

It is possible to concentrate precursor ion signal into fewer charge states by IIPT reactions. These reactions are also useful for simplifying complex spectra of highly-charged species by spreading the ion signal over a larger analytical range (21, 22). In this dissertation, IIPT reactions are employed after ETD to reduce the charge of the ETD product ions. After proteins are fragmented by ETD, ion signal can cluster in a narrow m/z range, giving a

very complex spectrum with overlapping signals. For ETD product ions with various masses but similar m/z identities, IIPT will separate these signals by reducing the charge and shifting the m/z values (21, 22).

1.5.3 Ion/ion reaction kinetics

For anions and cations to react in the gas phase, the reactants need to come into close enough proximity that they form a stable orbiting complex with each other. The probability of this happening is approximated by the cross section (σ) formulated by Thomson's classical model for a three-body interaction:

$$\sigma \approx \frac{Z_1^2 Z_2^2 e^4}{\varepsilon_0 (\mu v^2)^2} \qquad (1.7)$$

in which Z_1 and Z_2 are the charges of the reacting species, e is the elementary charge, ε_0 is the vacuum permittivity, μ is the reduced mass, and v is the relative velocity between the reacting species.

The overall ion/ion reaction rates are determined by the rate constant k, which is a function of the ion/ion reaction cross section of the relative velocity of the reactants:

$$k \propto v\left(\frac{Z_1^2 Z_2^2 e^4}{\varepsilon_0 (\mu v^2)^2}\right). \quad (1.8)$$

Determining the spatial and temporal overlap and number densities of the ion clouds make directly measuring k an arduous task. Fortunately, typical ion/ion reaction conditions use a large excess of the singly charged reagent anion to create pseudo first order kinetics in the precursor cation. The dependence of the reaction rate on the reaction cross section is still observed experimentally under pseudo first order conditions through the rate dependence on reactant's charge state. Stephenson and McLuckey observed that the reaction rate correlates directly with the square of the precursor's charge state; the more highly charged the precursor, the faster the ion/ion reaction (22, 23).

1.5.4 Ion Parking during ion/ion reactions

Equation 1.8 models that the reaction cross section is inversely proportional to the relative velocity between the reaction partners. McLuckey and colleagues exploited this relationship to develop a technique called "ion parking" for ion/ion reactions. These investigators superposed a single supplemental AC potential to an AC-only ion trap to specifically resonantly kinetically excite a single ion during an ion/ion reaction. Since the relative

velocity between that ion and reagent then increased, a drastically reduced ion/ion reaction rate resulted (24,26). The excited ion appeared unreactive, or simply "parked."

1.6 Challenges in characterizing intact proteins

Primary structure interrogation of proteins by MS/MS typically starts with proteolytic degradation of the protein into smaller peptides; it is these peptides that are actually analyzed. Although this approach has repeatedly been proven a valuable tool in recent decades, the amount of biological information accessible has been limited. Typical proteolytic degradation results in a complex mixture of peptides of varying sizes. Smaller peptides are often lost during fractionation, generating an incomplete picture of the protein. This makes it difficult to identify isoforms, splice variants, and mutations. Post-translational modifications are often cooperative between protein subunits; determining the exact biological implications requires detecting modifications within the context of one another. Additionally, proteolysis is usually accomplished with enzymatic digestion. This process can be time-intensive and introduces the potential for contamination. In contrast,

characterizing an intact protein would lead to unambiguous assignment of its identity and a comprehensive picture of all modifications that co-exist on all proteoforms of the protein in vivo, with minimal manual sample preparation. Determining primary structure of intact proteins is complicated by the limited production of fragment ions, difficulties in efficiently restricting the fragmentation into desirable channels, and spectral complexity from the diversity of fragment ions.

Intact proteins have many more fragmentation channels than peptides. For example, a 10mer peptide like angiotensin II can dissociate at 9 places on the peptide backbone to generate 18 possible fragment ions. A 153-residue protein like apomyoglobin will ideally only dissociate at 152 places to create 304 possible fragment ions. The many more possible dissociation channels means that for the same given number of precursor ions, the fragment ion signal is diluted significantly. However, the maximum storage capacity for LITs is 1.0E6 charges, not ions (5, 8). For a 1.0E6 target, the maximum precursor population for a peptide with 4 charges is about 2.5E5 ions. In contrast, a protein precursor with 20 charges has starting population of about

5.0E4 ions. So not only do proteins have diluted fragment ion signal due to the increased number of possible dissociations, there are significantly fewer precursor ions. This unfortunate combination restricts production of fragment ions.

Since fragment ion signal is limited, the ideal dissociation method would efficiently direct all fragment ion signal into sequence-informative channels. However, most dissociation methods have limitations in this respect. Small molecule losses, most commonly water and ammonia, and losses of labile modifications are frequently observed with collisional-based dissociation methods. Electronic excitation, such as ultra violet photodissociation, will fragment every bond in the peptide backbone, as well as in the side chain (27). This creates too diverse a fragment ion population to be efficient. Intact proteins are very prone to secondary ETD reactions, generating internal fragments that are not sequence informative; this is discussed in greater detail in Chapter 4 of this dissertation.

Lastly, the resolution requirements for deciphering the complex spectra of intact protein MS/MS analysis are strenuous. Intact proteins are much

more likely generate fragments with overlapping m/z signals. In the comparison of angiotensin II to apomyoglobin, angiotensin II's 18 possible fragment ions are less likely to have overlapping m/z signals than apomyoglobin's 304 possible fragment ions. Even with subsequent employment of IIPT after fragmentation to spread the fragment ion signal through the mass spectrometer's analytical range, the large numbers of fragment ions can still create crowded signals (28–30).

1.7 Conclusions

The unifying focus of this research is improving MS capabilities to analyze intact proteins through new innovations in ion/ion reactions. Achievement of these goals would allow rapid, complete characterization of all PTMs and identification of isoforms, splice variants, and mutations. This information could open avenues of biological interrogation that previously had limited or no analytical capabilities for investigation.

This goal is explored in Chapter 2 by employing technology previously developed in the Hunt Laboratory to determine the primary structure of clinically relevant intact proteins; namely, the use of sequential ion/ion

reactions (ETD followed by IIPT) and accumulation of product ions from multiple iterations of fragmentation in the C-trap allowed for identification of hemoglobin variants. Chapter 3 explores the physics of ion motion during an ion/ion reaction in a quadrupole ion trap, discoveries which were integral to the applications presented in Chapter 4. Chapter 4 is describes a novel method to extend sequence coverage of intact proteins through selective control of ion/ion reaction kinetics.

1.8 References

1. Smith LM, Kelleher NL (2013) Proteoform: a single term describing protein complexity. Nat Methods 10(3):186–187.
2. Steen H, Mann M (2004) The abc's (and xyz's) of peptide sequencing. Nat Rev Mol Cell Biol 5(9):699–711.
3. Earley L, et al. (2013) Front-end electron transfer dissociation: A new ionization source. Anal Chem 85(17):8385–8390.
4. Banerjee S, Mazumdar S (2012) Electrospray Ionization Mass Spectrometry: A Technique to Access the Information beyond the Molecular Weight of the Analyte. Int J Anal Chem 2012:1–40.
5. Schwartz JC, Syka JEP, Quarmby ST (2010) Differential-pressure dual ion trap mass analyzer and methods of use thereof. Available at: https://patents.google.com/patent/US7692142B2/en.
6. Pekar Second T, et al. (2009) Dual-Pressure Linear Ion Trap Mass Spectrometer Improving the Analysis of Complex Protein Mixtures. Anal Chem 81(18):7757–7765.
7. Eliuk S, Makarov A (2015) Evolution of Orbitrap Mass Spectrometry Instrumentation. Annu Rev Anal Chem 8(1):61–80.
8. Schwartz JC, Senko MW, Syka JEP (2002) A Two-Dimensional Quadrupole Ion Trap Mass Spectrometer. J Am Soc Mass Spectrom 13(02):659–669.
9. Schwartz JC, Syka JEP (2004) Two-Dimensional Quadrupole Ion Trap

Operated as a Mass Spectrometer.

10. Douglas DJ, Frank AJ, Mao D (2005) Linear ion traps in mass spectrometry. Mass Spectrom Rev 24(1):1–29.
11. Snyder DT, Peng WP, Cooks RG (2017) Resonance methods in quadrupole ion traps. Chem Phys Lett 668:69–89.
12. March RE, Todd JFJ (2005) Quadrupole Ion Trap Mass Spectrometry (John Wiley & Sons, Inc). 2nd Ed. doi:10.1002/0471717983.
13. Williams JD, et al. (1994) Resonance Ejection Ion Trap Mass Spectrometry and Nonlinear Field Contributions: The Effect of Scan Direction on Mass Resolution. Anal Chem 66(5):725–729.
14. Gunawardena HP, et al. (2005) Electron Transfer versus Proton Transfer in Gas-Phase Ion/Ion Reactions of Polyprotonated Peptides. J Am Chem Soc 127(36):12627–12639.
15. Syka JEP, Coon JJ, Schroeder MJ, Shabanowitz J, Hunt DF (2004) Peptide and protein sequence analysis by electron transfer dissociation mass spectrometry. Proc Natl Acad Sci 101(26):9528–9533.
16. Ledvina AR, et al. (2010) Activated-Ion Electron Transfer Dissociation Improves the Ability of Electron Transfer Dissociation to Identify Peptides in a Complex Mixture. Anal Chem 82(24):10068–10074.
17. Turecˇek F, et al. (2010) The Histidine Effect. Electron Transfer and Capture Cause Different Dissociations and Rearrangements of Histidine Peptide Cation-Radicals. J Am Chem Soc 132(31):10728–10740.
18. Liu J, McLuckey SA (2012) Electron transfer dissociation: Effects of cation

charge state on product partitioning in ion/ion electron transfer to multiply protonated polypeptides. Int J Mass Spectrom 330–332:174–181.

19. Compton PD, Strukl J V., Bai DL, Shabanowitz J, Hunt DF (2012) Optimization of electron transfer dissociation via informed selection of reagents and operating parameters. Anal Chem 84(3):1781–1785.
20. Prentice BM, McLuckey SA (2013) Gas-phase ion/ion reactions of peptides and proteins: acid/base, redox, and covalent chemistries. Chem Commun 49(10):947–965.
21. Coon JJ, et al. (2005) Protein identification using sequential ion/ion reactions and tandem mass spectrometry. Proc Natl Acad Sci 102(27):9463–9468.
22. McLuckey SA, Huang TY (2009) Ion/ion reactions: New chemistry for analytical MS. Anal Chem 81(21):8669–8676.
23. McLuckey SA, Stephenson JL (1998) Ion/ion chemistry of high-mass multiply charged ions. Mass Spectrom Rev 17(6):369–407.
24. Chrisman PA, Pitteri SJ, McLuckey SA (2005) Parallel Ion Parking: Improving Conversion of Parents to First-Generation Products in Electron Transfer Dissociation. Anal Chem 77(10):3411–3414.
25. McLuckey SA, Reid GE, Wells JM (2002) Ion Parking during Ion/Ion Reactions in Electrodynamic Ion Traps. Anal Chem 74(2):336–346.
26. Chrisman PA, Pitteri SJ, McLuckey SA (2006) Parallel Ion Parking of Protein Mixtures. Anal Chem 78(1):310–316.

27. Holden DD, McGee WM, Brodbelt JS (2016) Integration of Ultraviolet Photodissociation with Proton Transfer Reactions and Ion Parking for Analysis of Intact Proteins. Anal Chem 88(1):1008–1016.
28. Garcia BA (2010) What does the future hold for top down mass spectrometry? J Am Soc Mass Spectrom 21(2):193–202.
29. Gregorich ZR, Ge Y (2014) Top-down proteomics in health and disease: Challenges and opportunities. Proteomics 14(10):1195–1210.
30. Weisbrod CR, et al. (2017) Front-End Electron Transfer Dissociation Coupled to a 21 Tesla FT-ICR Mass Spectrometer for Intact Protein Sequence Analysis. J Am Soc Mass Spectrom 28(9):1787–1795.

Chapter 2

2. Analysis of Hemoglobin Variants Using Novel Mass Spectrometric Techniques for Intact Protein Interrogation

This project is a collaboration with Drs. Dave Herold and Jane Yang at University of California San Diego.

2.1 Overview

Hemoglobin is a tetrameric proteins responsible for transporting oxygen from the lungs to tissues through the bloodstream. Hemoglobinopathies, disorders in which a hemoglobin subunit contains one or more amino acid substitutions, can have severe effects on a person's health. Presented here is a straightforward MS/MS method for primary structure evaluation of the intact hemoglobin subunits. The samples selected for this study had discrepant or no identification in clinical analyses by capillary zone electrophoresis and high pressure liquid chromatography. In conjunction with multiple fills of the product ions into the C-trap prior to Orbitrap analysis, it is demonstrated that using electron transfer dissociation reactions followed by ion/ion proton transfer reactions when analyzing the intact hemoglobin subunit is sufficient to confidently identify hemoglobin variants. Additionally, an MS/MS/MS method is described that identified a previously unknown hemoglobin variant, which is now identified as Hemoglobin Charlottesville.

Chapter 2

2.2 Introduction

2.2.1 Hemoglobin

Hemoglobin (Hb) is a multi-subunit metalloprotein responsible for binding oxygen cooperatively in the lungs, transporting the oxygen through the blood, and releasing the oxygen in peripheral tissues to support oxidative metabolic processes. Each subunit is complexed around an iron-containing heme, as seen in Figure 2.1. Four of the ferrous atom's six coordination sites are occupied by the porphyrin ring, a fifth is occupied by a proximal histidine of the surrounding globin subunit, and the sixth reversibly binds oxygen (1).

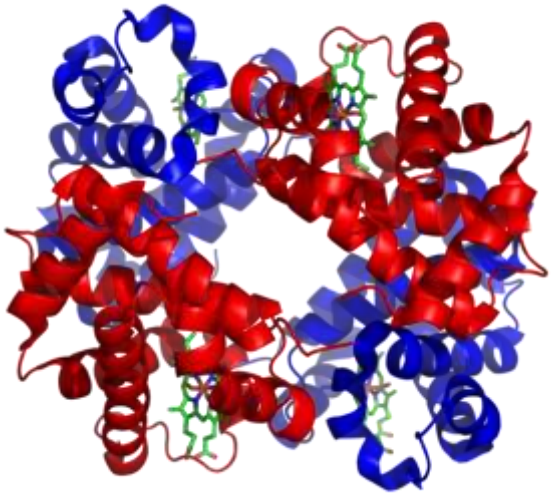

Figure 2.1. Hb A structure. The α-globin subunits are red, β-globin subunits are blue, and hemes are green. (PDB structure 1GZX)

Chapter 2

Adult human hemoglobin is primarily Hb A, a tetramer characterized by two α-globin and two β-globin subunits. These are encoded by the duplicated HBA1 and HBA2 genes and by the HBB gene, respectively(1). The α-globin subunit is 15.1 kDa (141 residues), while the β-globin subunit is a slightly larger 15.8 kDa (146 residues.)

2.2.2 Hemoglobinopathies

The HBA1 and HBA2 genes commonly contain single nucleotide polymorphisms that result in single amino acid substitutions to the transcribed globin subunits, creating hemoglobin variants. The resulting hemoglobin disorders, or hemoglobinopathies are the most common inherited disorder; it is estimated that 150 million people worldwide carry a variant Hb gene (1). While most of these variants have little or no physiological manifestations, some variants can have drastic effects on the structure and function of the Hb molecule.

A common hemoglobin variant, Hb S, substitutes valine for glutamic acid at position 6 (E6V) on the β-globin chain. These variants ultimately

causes the red blood cell distort into a crescent, sickle shape and break down prematurely, leading to a condition known sickle cell anemia (2). Hb E is a β-globin chain E26K variant that causes small and irregularly shaped red blood cells, leading to mild anemia (2, 3). To avoid clinical complications and promote prophylactic care, neonatal screening for hemoglobinopathies is routine in the United States (4).

2.2.3 Current methods for identifying hemoglobin variants

Linus Pauling's 1949 seminal work with sickle cell anemia patients first identified the existence of variant Hb molecules through a difference in electrophoretic mobility relative to normal Hb molecules (5). Over 1600 Hb variants have since been identified, although most have no physiological manifestations (6) The primary method for identifying Hb variants has been electrophoresis, which separates molecules based on charge differences in a pH-controlled environment (7). Chromatographic methods, such as reverse phase and cation exchange high pressure liquid chromatography (RP-HPLC and CE-HPLC, respectively) have also been widely used. Separation is based on the Hb molecule's hydrophobicity in RP-HPLC. For CE-HPLC, separation

depends on the Hb variant's affinity for the negatively charged stationary phase (7).

Although separation techniques are standard methods for detecting variants, they are often insufficient to definitively identify the variant (7). Separation methods rely on the variation to induce a significant physicochemical change. For example, electrophoretic methods only identify variants with an abnormal number of ionizable amino acids; since only 5 of the 20 amino acids are ionizable, many Hb variants are missed. Additionally, these methods do not provide direct primary structure information that identifies the position of the mutation.

For clinical purposes, typical variant screening compares a separation profile against a library of separation profiles of known, common variants. Frequently, clinical screening for Hb variants is a two-tiered process employing two different analytical techniques, generally RP-HPLC and capillary electrophoresis (3, 4). These methods routinely disagree on variant identification (8, 9), requiring further evaluations, principally through DNA sequencing.

2.2.4 Mass spectrometric analysis of hemoglobin variants

Many MS methods for analyzing Hb variants have been developed to utilize mass spectrometry's high degree of specificity, primarily through MS/MS analysis after proteolytic degradation (1, 10). A variant can be determined through the mass change due to substituted amino acid; this allows for identification of a variant regardless of changes in physicochemical properties. However, methods analyzing the intact globin subunits by MS/MS are particularly attractive. Speed is a priority when screening clinical samples, so analyzing the intact globin subunit eliminates the need for strenuous sample preparation and can still pinpoint the site of the substituted amino acid.

The direct analysis of intact globin chains by MS/MS is not routinely applied for Hb variant analysis. Such a large protein will fragment into many, many different ions; this creates a complex spectrum with overlapping signals that can be difficult to interpret. Additionally, larger fragments inherently have a lower signal-to-noise ratio due to the dilution of signal into multiple isotopes. Smaller fragments are preferentially identified, such that the primary

information recovered are limited to the sequences near the N- or C-termini. Edwards et al. were able to use collisional fragmentation of the intact β-globin subunit to identify Hb C, Hb D, and Hb S; these mutations (E6K, E121Q, and E6V, respectively) are all near the protein termini (10). A β-globin variant, S72R, was identified by Edwards et al. using a combination of CID and ETD, which provided 46% and 34% sequence coverage, respectively; the combined sequence coverage from this dual analysis was 63%(11).

In many methods for MS/MS analysis of the intact globin subunits, it was necessary to identify diagnostic product ions, or fragment ions that reveal structural or compositional information about its precursor ion. These are ions that are expected to form in the fragmentation of non-mutant globin subunits, as pre-determined empirically for that method of analysis. If the diagnostic ions are not observed, it indicates the presence of a variant. Graca et al. used 50 diagnostic ETD product ions to identify rare Hb variants, Hb G-Siriraj, Hb E, Hb O-Arab, and Hb Inglewood (E7K, E26K, E121K, and A142T β-globin variants, respectively)(12). Mekecha et al. characterized potential diagnostic ions for collisional induced fragmentation of α- and β-globin

variants, a work challenged by the critical dependence of fragmentation pathways on precursor charge state (13).

In this work, we present identification of 19 Hb variants by ETD/IIPT LC-MS/MS analysis; these clinical samples had discrepant or no identifications from capillary zone electrophoresis (CZE) and HPLC analyses. The variant amino acids are on either the α-, β-, or both the α- and β-globin subunits with mass differences from 0.0364 to 99.0796 Da. The variation positions are not localized to the protein termini, which would have precluded their identification with previous mass spectrometric techniques. Additionally, we present a previously unidentified Hb variant, Hb Charlottesville, an α-globin S138X variant (X=I or L.)

2.3 Materials, Equipment, and Instrumentation

Agilent Technologies (Palo Alto, CA)

1100 Series High Performance Liquid Chromatograph

1100 Series Vacuum Degasser

POROSHELL 300SB-C18 resin (5-μm, 300-Å)

POROSHELL 300SB-C8 resin (5-μm, 300-Å)

Chapter 2

POROSHELL 300SB-C3 resin (5-µm, 300-Å)

Eppendorf (Hauppauge, NY)

5414R Benchtop centrifuge

Fisher Scientific (Hampton, NH)

Tris(2-carboxyethyl)phosphine hydrochloride (TCEP•HCl)

Honeywell (Morristown, NJ)

Burdick and Jackson™ Acetonitrile, LC-MS grade

Molex (Lisle, IL)

Polymicro Technologies™ polyimide coated fused silica capillary, 360 µm o.d. x 75 µm i.d. and 360 µm o.d. x 100 µm i.d.

New Objective (Woburn, MA)

PicoClear™ Union Assembly

Oakwood Chemical (Estill, SC)

Perfluoromethyldecalin

PQ Corporation (Valley Forge, PA)

Kasil – Potassium silicate solution

Sigma Aldrich (St. Louis, MO)

2-butanone

Ammonium hydroxide

Fluoranthene, >99% purity

N-(2-aminoethyl)maleimide trifluoroacetate salt

Sutter Instrument Co. (Navato, CA)

P-2000 microcapillary laser puller

Thermo Fisher Scientific (San Jose, CA; Bremen, Germany)

Orbitrap Elite™ Hybrid Ion Trap-Orbitrap Mass Spectrometer

Formic Acid, LC-MS Grade

Pierce Water, LC-MS Grade

Urea

2.4 Methods

2.4.1 Sample Preparation

Whole blood was washed three times in saline by Jane Yang at University of California San Diego. The cells in the whole blood sample were lysed by freezing; the frozen samples were shipped to the Hunt Laboratory at University of Virginia.

Chapter 2

For all samples, 100 microliters of the whole blood lysate were diluted 200 fold in water, vortexed, and centrifuged for 10 min at 14k rcf for 10 minutes. The sample was transferred to a new tube, and the pellet was discarded.

For samples containing Hb Charlottesville and both Hb Athens-Georgia samples, 5 uL of the Hb sample was diluted to approximately 1 pmol/uL with 995 uL of 0.1% acetic acid in water. For Hb Ty Gard, Hb G-Philadelphia/ Hb S and Hb N-Baltimore 50 uL of the Hb sample was diluted with 950 uL of 0.1% acetic acid to an approximate final concentration of 10 pmol/uL.

For the remaining samples, the heme was removed from the red blood cell lysate. To do this, 2 uL of 5% hydrochloric acid in water and 200 uL of 2-butanone were added to the sample. The sample was briefly vortexed and centrifuged for 5 minutes at 14k rcf. The heme-containing supernatant was discarded, and the aqueous layer was transferred to a new tube.

For Hb Atlanta, HB Coombe Park, and Hb J-Habana, 200 uL of ethyl acetate was added, vortexed briefly, and centrifuged for 10 minutes at 14k rcf to remove any remaining cell membrane. The organic supernatant was subsequently discarded, and the sample was transferred to a new tube.

For the apohemoglobin samples containing Hb J-Cairo and Hb Masuda, 50 uL of the sample as prepared above was diluted with 700 uL of 0.1% acetic acid for an approximate final concentration of 10 pmol/uL. For the remaining apohemoglobin samples, 5 uL were diluted with 745 uL of 0.1% acetic acid in water to an approximate final concentration of 1 pmol/uL.

2.4.2 Reduction and alkylation with N-(2-aminoethyl)maleimide

Samples containing Hb J-Cairo, Hb Ty Gard, Hb N-Baltimore, Hb Masuda, and Hb G-Philadelphia/Hb S were treated to reduce any disulfide bonds, then the free cysteines were alkylated with N-(2-aminoethyl)maleimide (NAEM).

A 200 mM tris(2-carboxyethyl)phosphine (TCEP) solution was prepared in a 0.5% acetic acid/8 M urea in water solution. Ten microliters of the 10 pmol/uL hemoglobin sample was combined with 10 uL the 200 mM TCEP solution and incubated at 50°C for 10 minutes. This reduction reaction was quenched by adding enough 0.2M ammonium hydroxide such that the final pH was between 6.7 and 7.1 (approximately 7.5 uL.) Subsequently, 10 uL of a 30 mM NAEM solution prepared in 50mM ammonium acetate was added to the sample. After 10 minutes at room temperature, 4 uL of 25% formic acid

was added to the sample for an approximate final concentration of 2.4 pmol/uL.

2.4.3 On-line RP-HPLC separation for MS/MS analysis

One microliter of the 1pmol/uL of red blood cell lysate as prepared above was pressure loaded onto a 360x100-um i.d. fused silica Kasil-fritted micro-capillary guard column. For the reduced and NAEM alkylated samples, about 0.5 uL of the 2.4 pmol/uL solution was loaded. The guard column was washed with ~30 column volumes of 0.3% formic acid in water, then connected by a PicoClear™ union to a 360x75-um i.d. fused silica micro-capillary analytical column equipped with a laser-pulled electrospray emitter tip.

Various resins for RP-HPLC separation were used, in efforts to optimize separation of the globin subunits. In the initial stages of this study, C18 resins were used; resins with shorter aliphatic chains were later evaluated and discovered to promote separation of the globin subunits. For samples containing Hb Ty Gard, Hb Charlottesville, Hb G-Philadelphia/ Hb S, both Hb Athens-Georgia, and Hb Russ, both the guard and analytical columns were

packed with POROSHELL 300SB-C18 resin. For samples containing Hb N-Baltimore, Hb Lamentin, Hb Queens, Hb Atlanta, Hb Hopkins II, and Hb Enfield, the guard column was packed with POROSHELL 300SB-C8 resin, and the analytical column contained POROSHELL 300SB-C3. The guard and analytical columns for the remaining samples were packed with POROSHELL 300SB-C3 resin.

Samples containing Hb Ty Gard, Hb Charlottesville, Hb G-Philadelphia/ Hb S were eluted at 50 nL/min using a 0-30% B for 5 minutes, 30-70% B for 20 minutes, 70-100% B for 10 minutes (A= 0.3% formic acid in water; B= 0.3% formic acid, 72% acetonitrile, 18% isopropanol and 9.7% water, all v/v.)

The remaining samples were eluted at 50 nL/min using the gradient 0-40% B for 5 minutes, 40-45% B for 40 minutes, 45-100% B for 5 minutes (Solvent A: 0.3% formic acid in water; Solvent B: 0.3% formic acid, 72% acetonitrile, 18% isopropanol and 9.7% water, all v/v.)

2.4.4 MS and MS/MS analysis

The sample was ionized by microelectrospray as eluting off the

analytical column into the front end of an Orbitrap Elite™, which was modified in-house with a front-end reagent source for ETD and IIPT.

Samples were initially screened with HPLC-MS analysis of the intact globin subunits to identify the existence of the variants in the sample. These analyses used high-resolution full MS1 scans in the Orbitrap mass analyzer, which was followed by a low-resolution full MS scan in the low pressure cell of the linear ion trap. Orbitrap MS scan parameters were set as follows: r=120,000 at 400 m/z, 500-2000 m/z scan range, 1e5 ion count FTMS automatic gain control (AGC) target, and 1 microscan. The LIT MS scan parameters were as follows: 500-2000 m/z scan range, 3e4 precursor IT AGC target, 3e5 reagent AGC target, and "normal" scan rate.

Ions of the variant subunit of the highest charge state that also had reasonable abundance were identified and used as targets in a second analysis of the sample, a targeted HPLC-MS/MS experiment. The samples were once again separated by HPLC, and the targeted ions of the variant subunit were isolated, fragmented by ETD, followed by charge-reducing IIPT. The MS/MS scan parameters were set as follows: resolution (r) =120,000 at

400 m/z, 500-2000 m/z scan range, 1e5 ion counts FTMSn AGC target, 3e5 ion counts reagent AGC target, 10 fragment ion fills into the C-trap, 1 microscan, 5 m/z precursor isolation window, 7-12 ms ETD, and 7-10 ms IIPT.

The MS and MS/MS spectra were examined using Qual Browser software (Thermo Fisher Scientific.) Interpretation of the ETD/IIPT MS/MS was performed manually on the unprocessed raw spectra, averaging 5-10 MS/MS spectra. Percent sequence coverage was calculated by dividing the number of the observed N-C_α bond cleavages by the total numbers of predicted N-C_α bond cleavages. Although cleavage of the N-C_α bond that is N-terminal to proline does not produce an observable fragment, it is counted as a missed cleavage to not artificially inflate sequence coverage. Masses for all intact fragments identified were within 5 ppm of the predicted masses, as calculated by an in-house fragment mass calculator.

Chapter 2

2.5 Results

2.5.1 Novel methods for intact protein analysis

Two novel methods previously developed in the Hunt Laboratory were employed for analyzing the hemoglobin variant subunits: sequential use of ETD and IIPT and multiple fills of the ion/ion reactions' product ions into the C-trap.

Short ETD reaction times were selected to reduce secondary fragmentation of the ETD product ions as much as possible, which allows for more interpretable sequence ions containing the N- or C-terminus. However, this concentrates the fragment ion signals into a narrow domain around the precursor m/z which results in multiple overlapping product ion isotopic distributions; the complexity of the product ion spectrum in this region requires high resolving power. The subsequent employment of IIPT after ETD circumvents this strenuous resolution requirement. IIPT reduces the charge of the ETD fragment ions, moving the ions' m/z identity throughout the analytical m/z range. This reduction of spectral complexity allows for ion identification at moderate resolving power (15,16).

Accruing a large product ion population before analysis has been shown to offset the loss of signal from the concomitant charge reduction of ion/ion reactions. Software modifications to this analytical system allow for multiple iterations of ion/ion reaction productions to be accumulated in the C-trap. These accumulated ions are then transferred en masse to the Orbitrap for mass analysis. This approach has been proven to improve mass spectral signal-to-noise ratio, dynamic range, and scan rate (16).

2.5.2 Identification of Hb variants

The hemoglobin samples were initially screened by RP-HPLC-MS; the exact conditions vary as described in 2.4.3 as conditions were optimized for separation of the globin subunits. Once the variant was identified in the screen, the sample was re-analyzed via targeted RP-HPLC-MS/MS with ETD/IIPT enabled with multiple C-trap fills of the product ions; a charge state of the variant of sufficient abundance and charge density was selected from the screen as the target precursor ion. The hemoglobin variants identified are

presented in Table 2.1. The sample containing both an α- and β-globin variant is examined in greater detail below.

One sample contained two variant globin chains, Hb G-Philadelphia (N68K α-globin variant) and Hb S. An elution profile for the 4 major species in this sample can be seen in Figure 2.2: α-globin, N68K α-globin variant, β-globin, and β-globin E6V variant. The presence of all four globin chains confirms this sample is heterozygous for both the α- and β-globin subunits.

Chapter 2

Hemoglobin Variant	Variant subunit	Variation	Mass shift of variation
*Hb G-Philadelphia Hb S	α-globin β-globin	N68K E6V	+14 Da -30 Da
Hb J-Cairo	β-globin	K65Q	<1 Da
Hb N-Baltimore	β-globin	K95E	+1 Da
Hb Atlanta	β-globin	L75P	-16 Da
Hb Hopkins II	β-globin	H112D	-22 Da
**Hb Athens-Georgia	β-globin	R40K	-28 Da
Hb Taradale	β-globin	K82R	+28 Da
Hb Ty Gard	β-globin	P124Q	+31
Hb J-Baltimore	β-globin	G16D	+58 Da
Hb Tripoli	β-globin	E26A	-58 Da
Hb Masuda	β-globin	G119D	+58 Da
Hb Coombe Park	α-globin	K127E	+1 Da
**Hb Enfield	α-globin	H89Q	-9 Da
Hb Lamentin	α-globin	H20Q	-9 Da
Hb Queens	α-globin	L34R	+43 Da
Hb J-Toronto	α-globin	A5D	+44 Da
Hb J-Habana	α-globin	A71E	+58 Da
Hb Russ	α-globin	G51R	+99 Da

*This sample contained two hemoglobin variants.

**Two samples were identified with this hemoglobin variant.

Table 2.1. Hemoglobin variants detected by ETD/IIPT MS/MS analysis of globin intact subunits.

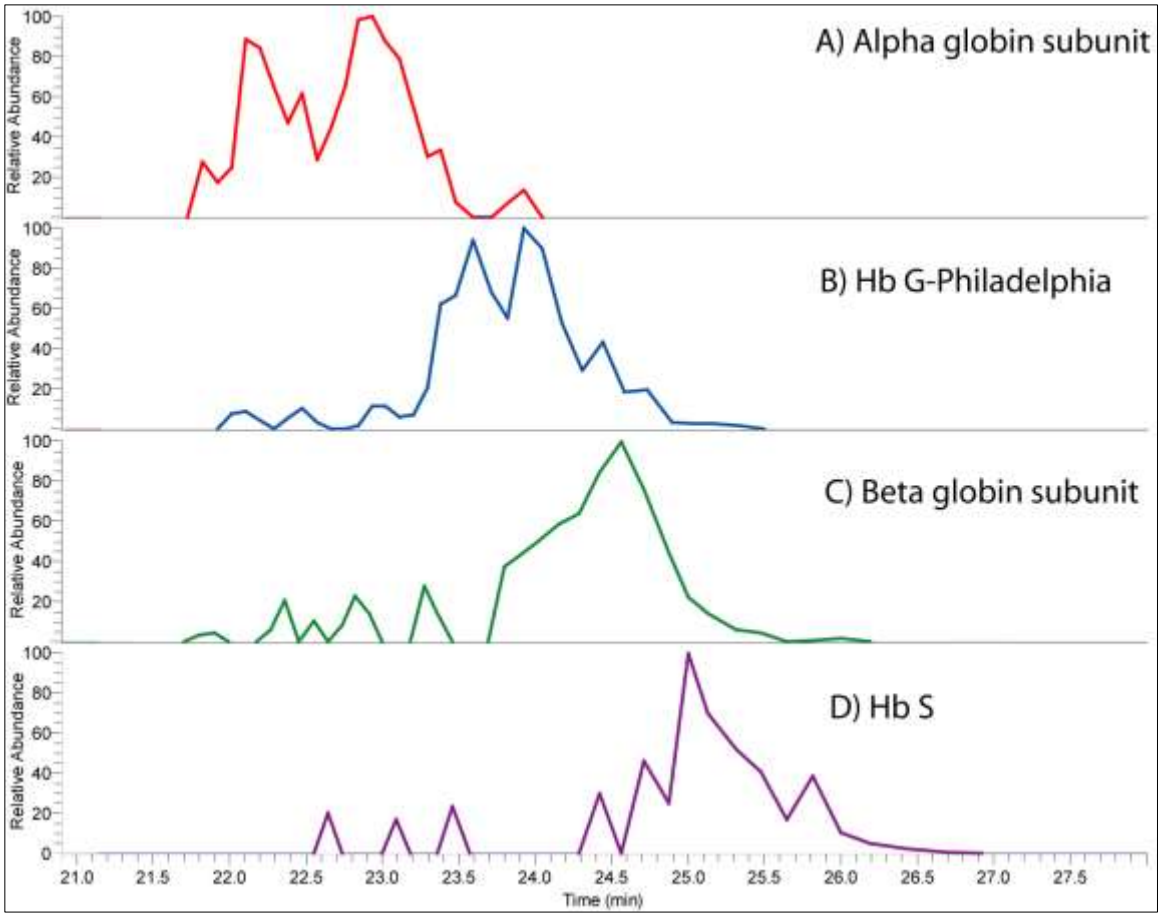

Figure 2.2. LC-MS elution profile of hemoglobin variant clinical sample with normal α-globin subunit (A), α-globin variant Hb G-Philadelphia (B), β-globin subunit (C), and β-globin variant Hb S.

Note the overlapping elution profile leads to a complicated spectrum with multiple co-eluting species. The $[M+20H]^{+20}$ of the α-globin variant and the $[M+21]^{+21H}$ of the β-globin variant were selected as precursor ions for MS/MS in a targeted analysis for 8ms ETD followed by 12 ms IIPT.

Chapter 2

The ETD/IIPT MS/MS spectrum for Hb G-Philadelphia is shown in Figure 2.3; the corresponding sequence coverage is shown in the inset. The intact mass of the precursor indicated a 14 Da increase in mass relative to the normal α-globin subunit. Fragment ions c_6-c_{67} and z_4-z_{73} show that the primary structure is unaffected in for the first 67 amino acids and the last 73 amino acids of the variant, respectively. Substituting lysine for N68 fits the expected 14 Da mass shift. Nine c-type ions and 14 z-type ions containing the N68K substitution were found, confirming the variant identity as Hb G-Philadelphia. The total sequence coverage by ETD/IIPT MS/MS was 76%.

The ETD/IIPT MS/MS spectrum and corresponding sequence coverage for Hb S is seen in Figure 2.4. From the intact mass of the precursor, a substitution that decreased the subunit's mass by 30 Da was expected. A single N-terminal containing fragment (c_5) was identified, but C-terminal containing fragments up to z_{86} were identified. This indicated that the variant was close to the N-terminus. Substituting valine for the glutamic acid at position 6 created a 30 Da deficit. Sixty-three fragment ions were identified with the E6V variation, cinching a conclusive identification of Hb S. The total sequence coverage was 73%.

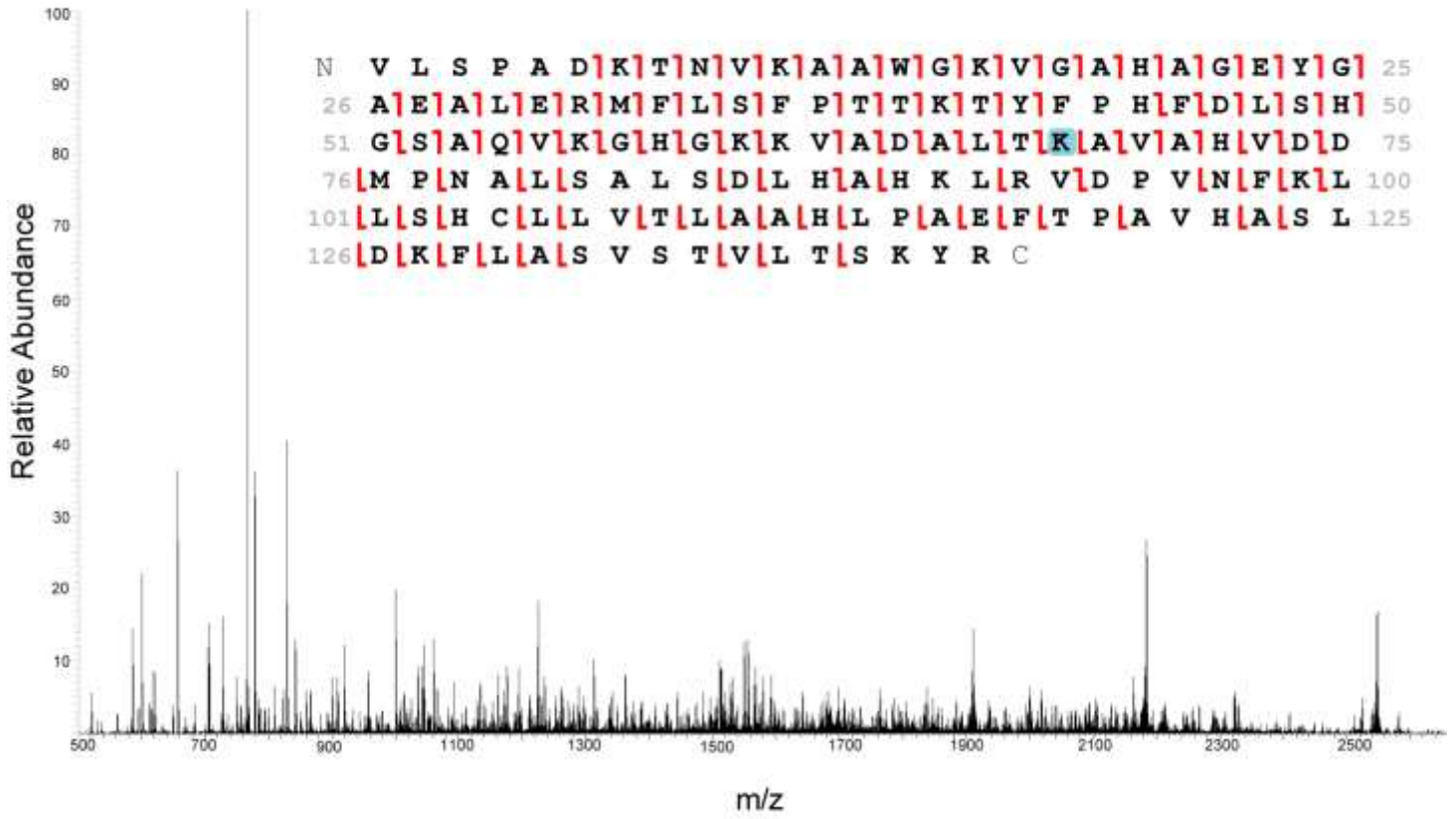

Figure 2.3. The ETD/IIPT spectrum of $[M+20H]^{+20}$ of Hb G-Philadelphia, an α-globin N68K variant. Inset: Sequence coverage of Hb G-Philadelphia from ETD/IIPT MS/MS analysis. Highlighted in blue is variant at position 68. In total, 130 fragments were identified.

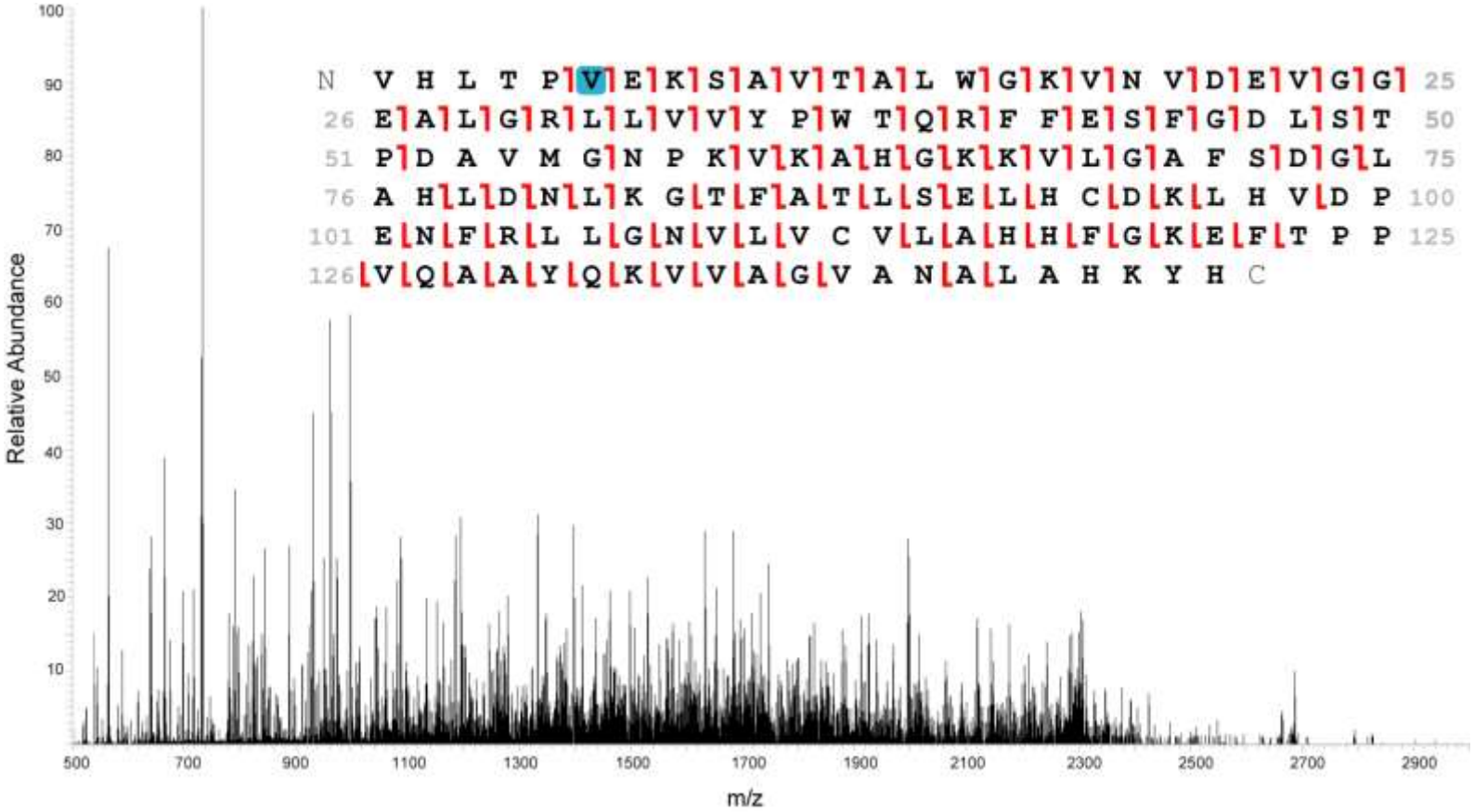

Figure 2.4. The ETD/IIPT spectrum of $[M+21H]^{+21}$ of Hb S, an β-globin E6V variant. Inset: Sequence coverage of Hb S from ETD/IIPT MS/MS analysis. Highlighted in blue is variant at position 6. In total, 118 fragments were identified.

containing fragments up to z_{86} were identified. This indicated that the variant was close to the N-terminus. Substituting valine for the glutamic acid at position 6 created a 30 Da deficit. Sixty-three fragment ions were identified with the E6V variation, cinching a conclusive identification of Hb S. The total sequence coverage was 73%.

Positive identification of the variants presented in Table 2.1 prove the utility of ETD/IIPT with multiple C-trap fills of the product ions prior to high resolution mass analysis. This method allows for robust and confident identification of sequence variants. The Hb variants identified are not all localized to the protein termini, such as Hb G-Philadelphia, Hb J-Cairo, or Hb J-Habana. The variations do not necessarily induce physiochemical changes, like Hb Athens-Georgia or Hb Taradale. The mass differences between variants ranges from 99 Da for Hb Russ to less than 1 Da for Hb J-Cairo, making the method applicable to a wide variety of Hb variants. Additionally, most variant identifications were accompanied by a large number of fragment ions containing the variation, leading to a highly confident assignment.

2.5.3 Hemoglobin Charlottesville

During the course of this work, one Hb sample contained a variant α-globin subunit that displayed a 26 Da increase in mass. When analyzed by MS/MS with ETD/IIPT (spectrum shown in Figure2.5A), a serine→X (where X denotes either of the isobaric leucine or isoleucine amino acids) variation was localized to the C-terminus. However, the smallest C-terminal containing fragment ion recovered by ETD/IIPT was z_{11}, which contained the S→X variant. There are 3 serines on the C-terminus which could have potentially been substituted: S131, S133, and S138.

To definitively identify the variant, MS/MS/MS analysis was utilized. The alpha globin variant once again underwent ETD/IIPT, then only the z_{15}^{+2} product ion was transferred to the C-trap. After 15 iterations of ETD/IIPT, the accumulated z_{15} product ions were transferred to the HCD cell, where they were fragmented by collisions with the nitrogen bath gas to produce b- and y-type ions. After high resolution mass analysis (spectrum seen in Figure2.5B), the variation was localized to S138. This Hb variant had not been previously identified and received the name "Hb Charlottesville." Total sequence coverage of the combined MS/MS and MS/MS/MS analyses was 76% (Figure 2.5C.)

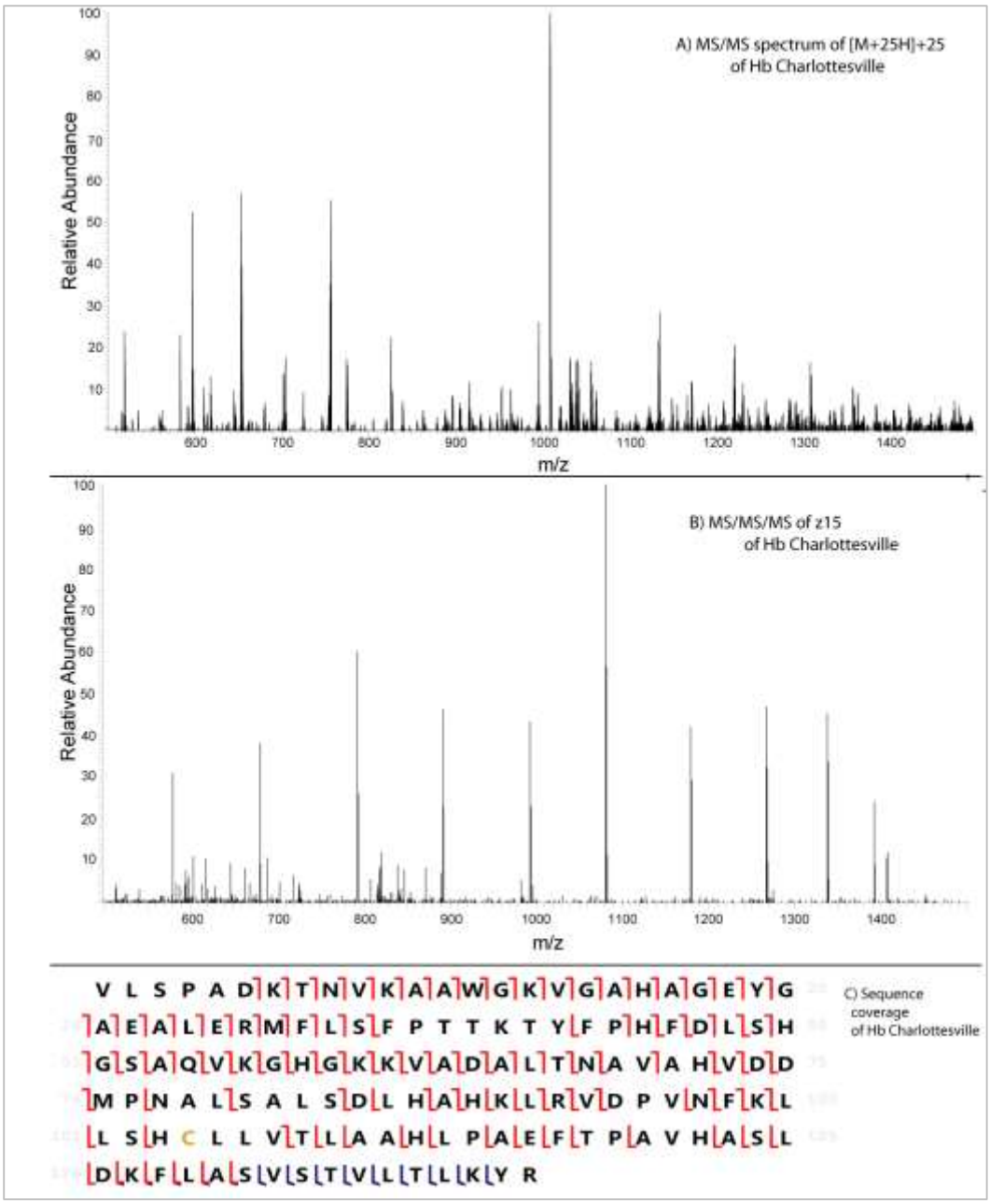

Figure 2.5. Analysis of α-globin variant Hemoglobin Charlottesville. A) ETD/IIPT spectrum of $[M+20H]^{+20}$ precursor of Hb Charlottesville. The z15 ion from this analysis was selected for further fragmentation in an MS/MS/MS experiment. B) The MS/MS/MS spectrum from higher energy collisional dissociation of the z15 ion. C) Sequence coverage of Hb Charlottesville. Sequence coverage obtained from MS/MS analysis is denoted by the c- and z-type ions in red. Sequence coverage obtained from MS/MS/MS analysis is denoted by the y-type ions in blue. In total, 145 fragments were identified.

Chapter 2

2.6 Conclusions

We have shown that ETD/IIPT analysis of intact globin subunits with multiple fills of product ions in the C-trap may be used for the diagnosis of unknown hemoglobin variants. Twenty-one clinical samples that were identified as variants by CZE and HPLC, but which could not by diagnosed by those methods, were analyzed; the identified variants are summarized in Table 2.1. The robustness of the method is shown by the diversity of variants identified. Variations were identified on the α- and β-globin subunits, independent of physicochemical changes, significant mass shifts, or positions relative to the termini of the protein. The high degree of sequence coverage enables confident diagnosis.

A MS/MS/MS strategy for difficult variant assignments is also presented, in which an abundant ETD/IIPT product ion was subjected to fragmentation by collisions with a heavy bath gas. This allowed for the identification of a previously unreported hemoglobin variant, an α-globin subunit S138X variant. To definitively identify this isobaric substitution (or substitution of the same mass,) the sample is currently being DNA sequenced.

Chapter 2

Further development of the methodology presented here requires automation of data analysis and improved RP-HPLC separation. Manual analysis of the MS/MS spectrum is time-consuming and inhibits the adoption of this method in clinical settings. Software capable of searching MS/MS spectra of proteins as large as intact globin subunits would need to be developed; ideally, the software would also include components to search against a database containing hemoglobin variants. Additionally, improvement of RP-HPLC to reduce co-elution of multiple globin subunits would allow for cleaner isolation of the precursor ions, reducing mixed MS/MS spectra of multiple precursors.

2.7 References

1. Thom CS, Dickson CF, Gell DA, Weiss MJ (2013) Hemoglobin Variants: Biochemical Properties and Clinical Correlates. Cold Spring Harb Perspect Med 3(3):a011858–a011858.
2. Mehta P (1995) Book Review Sickle Cell Disease: Basic principles and clinical practice Edited by Stephen H. Embury, Robert P. Hebbel, Narla Mohandas, and Martin H. Steinberg. 902 pp., illustrated. New York, Raven Press, 1994. $145. 0-7817-0142-2. N Engl J Med 332(6):403–403.
3. Upadhye DS, et al. (2016) Neonatal Screening and the Clinical Outcome in Children with Sickle Cell Disease in Central India. PLoS One 11(1):e0147081.
4. Pass KA, et al. (2000) US Newborn Screening System Guidelines II: Follow-up of Children, Diagnosis, Management, and Evaluation Statement of the Council of Regional Networks for Genetic Services (CORN). J Pediatr 137(4):S1–S47.
5. Pauling L, Itano HA, Singer SJ, Wells IC (1949) Sickle Cell Anemia, a Molecular Disease. Science (80-) 110(2865):543–548.
6. Giardine B, et al. (2014) Updates of the HbVar database of human hemoglobin variants and thalassemia mutations. Nucleic Acids Res 42(D1):D1063–D1069.
7. Clarke G, Higgins T (2000) Laboratory Investigation of Hemoglobinopathies and Thalassemias: Review and Update. Clin Chem 46(8):1284–1290.
8. Keren DF, Hedstrom D, Gulbranson R, Ou C-N, Bak R (2008) Comparison of Sebia Capillarys Capillary Electrophoresis With the Primus High-Pressure Liquid Chromatography in the Evaluation of Hemoglobinopathies. Am J Clin Pathol 130(5):824–831.
9. Degandt S, et al. (2018) Evaluation of four hemoglobin separation analyzers for hemoglobinopathy diagnosis. J Clin Lab Anal 32(1):e22224.
10. Brennan SO (2007) Fifty-Eight Years of Hemoglobin Analysis. Clin Chem 54(1):8–10.
11. Edwards RL, et al. (2011) Hemoglobin Variant Analysis via Direct Surface Sampling of Dried Blood Spots Coupled with High-Resolution Mass

Spectrometry. Anal Chem 83(6):2265–2270.

12. Edwards RL, Griffiths P, Bunch J, Cooper HJ (2012) Top-Down Proteomics and Direct Surface Sampling of Neonatal Dried Blood Spots: Diagnosis of Unknown Hemoglobin Variants. J Am Soc Mass Spectrom 23(11):1921–1930.
13. Coelho Graça D, et al. (2015) Identification of hemoglobin variants by top-down mass spectrometry using selected diagnostic product ions. Anal Bioanal Chem 407(10):2837–2845.
14. Mekecha TT, Amunugama R, McLuckey SA (2006) Ion Trap Collision-Induced Dissociation of Human Hemoglobin α-Chain Cations. J Am Soc Mass Spectrom 17(7):923–931.
15. Coon JJ, et al. (2005) Protein identification using sequential ion/ion reactions and tandem mass spectrometry. Proc Natl Acad Sci 102(27):9463–9468.
16. Weisbrod CR, et al. (2017) Front-End Electron Transfer Dissociation Coupled to a 21 Tesla FT-ICR Mass Spectrometer for Intact Protein Sequence Analysis. J Am Soc Mass Spectrom 28(9):1787–1795.

Chapter 3

3. Discoveries in Fundamental Ion Characteristics in Quadrupole Ion Trap During Ion/ion Reactions

This work was a collaborative effort with Drs. Chris Mullen and John EP Syka of ThermoFisher Scientific.

3.1 Overview

An ion's motion in a quadrupole ion trap is defined by its secular frequency of oscillation. Presented here is a novel method to characterize the physics of ion motion during mutual storage of both ion polarities. The presence of a negative electric field created by a dense anion cloud in the center of a quadrupole ion trap is shown to alter a precursor cation's secular frequency when simultaneously confined. The attractive potential created by the tightly constrained anion cloud decreases the cation's radial amplitude of oscillation, conferring a higher secular frequency to the cation than ideality. The anion's electric field is shown to neutralize expected secular frequency retardation from a self-space charged cation cloud. Increasing the volume of the anion cloud through resonant excitation is shown to alleviate the alteration of cation secular frequency

Chapter 3

3.2 Introduction

3.2.1 Motion of stored ions in a linear ion trap (LIT)

As discussed in 1.4.2, Ions will adopt characteristic, m/z-dependent secular frequencies of oscillation in the LIT. Therefore, the amplitude of oscillation varies directly with the ion's m/z. To acquire a high frequency of oscillation in a given period, small m/z ions oscillate quickly with smaller amplitude. Conversely, high m/z ions have a low frequency and large amplitude of oscillation (1). These amplitudes and frequencies are for both x- and y-planes of the LIT, but the motion is uncoupled. It can be useful to visualize ion motion in a quadrupolar field in which ion clouds are radially stratified into cylindrical layers, each layer for a specific m/z ion. Low m/z ion layers have smaller radii; large m/z ions have a larger radii (2).

The LIT confines a large number of ions in a low pressure environment, around 1E-4 torr. Ion/ion Coulombic interactions, especially in the absence of a dielectric medium, can become more significant as more ions are confined, such that space charging affect ion motion in the LIT (3). In the simplest case of self-space charge, Coulombic repulsion between large populations of closely-confined ions of like polarity forces the ion cloud to expand outward. An ion's secular frequency changes with its distance from the trap center.

Since the ion cloud now occupies different radial positions, the ions adopt new secular frequencies of oscillation in the trap. For self-space charging, the expanded ion cloud now has larger amplitudes of oscillation and therefore slower frequencies of oscillation (4, 5). The retarded frequencies can be observed by resonant ejection mass analysis as an apparent shift towards higher m/z values (6–9).

Mutual storage of large populations of anions and cations also affects the motion of the stored ions, although through Coulombic attraction between the ion clouds instead of repulsion within the clouds (10). Williams and Cooks observed improved peak shapes with resonance ejection of both space-charged anions and cations when ions of the opposite polarity were present in the trap, showing that the simultaneous confinement of both ion polarities can relieve self-space charging (11). Stephenson and McLuckey reported enhanced confinement of high m/z cations by using the attractive electric field created from space-charged, low m/z anions to augment pseudopotential well depths (12). These studies demonstrate the effects of simultaneous confinement of anions and cation, although the precise motion of the ions has not been experimentally investigated. Investigations of ion trajectories in quadrupole traps have been explored computationally;

however, these studies to date have focussed on single ion polarities and 3-D quadrupole ion traps.

3.2.2 Gas phase ion/ion reactions in the LIT follow pseudo first order kinetics of the precursor.

In 2004, the linear quadrupole ion trap was first used to simultaneously confine anions and cations (13). Important experimental considerations can impact both the efficiency and rates of ion/ion reactions in the LIT. Investigations by Compton et al. shortly after determined the optimal reagent Mathieu q_u, reaction times, and ion populations for optimal ETD in a LIT. To date, these conditions have remained the standard for ETD users (14). A summary of the optimal ion populations for ETD is presented below.

To maximize the rate and efficiency of the ETD reaction, the reagent anion is supplied in great excess. Typical ETD ion populations use 1E4 precursor cations and 3E5 reagent anions for LIT mass analysis. A higher precursor target of 1E5 is used for high resolution mass analysis due to the Orbitrap's higher spectral space charge limit. As the reagent anion has much smaller m/z, it is confined to a smaller volume within the ion trap. This causes the anion cloud to self-space charge and expand. This is necessary for

the radially stratified cation and anion clouds to interact; ion/ion reactions occur at the interface of the overlapping clouds. The expansion of the anion cloud due to self-space charging maximizes the overlap of the ion clouds so that the reaction rate remains constant for the duration of the reaction. These combined effects produce pseudo first order conditions for which can be written as

$$rate = k\,[cation][anion] = k'[cation] \qquad (3.1)$$

where [cation] and [anion] are the gas phase number densities of the two reactants. The pseudo rate constant k′ for this reaction is defined as

$$k' = k[anion]_0. \qquad (3.2)$$

Since ion densities are directly related to the Mathieu q_u of the ions, this parameter is held constant relative to the anion through the experiments presented in this chapter to ensure constant pseudo first order kinetics and a meaningful relative measurement of the reaction rate. This experimental consideration creates predictable reaction rates that scale directly with the square of the precursor charge state. Under such conditions, steady ion/ion reaction rates have been consistently observed (14).

The altered physics of cation motion during mutual storage of cations and anions under ETD conditions has not been previously characterized, but

this is the focus of this dissertation chapter. This is accomplished through use of a single frequency supplemental potential to "park" the precursor during the ion/ion reaction, as described in 1.5.4.

3.3 Materials, Equipment, and Instrumentation

Honeywell (Morristown, NJ)

Burdick and Jackson™ Acetonitrile, LC-MS grade

Molex (Lisle, IL)

Polymicro Technologies™ polyimide coated fused silica capillary, 360 µm o.d. x 75 µm i.d.

Sigma Aldrich (St. Louis, MO)

2,2′-biquinoline

Ubiquitin from bovine erythrocytes

Sutter Instrument Co. (Navato, CA)

P-2000 microcapillary laser puller

Tektronix (Beaverton, OR)

MDO3014 Mixed domain oscilloscope

ThermoFisher Scientific (San Jose, CA; Bremen, Germany)

Orbitrap™ Elite Hybrid Ion Trap-Orbitrap Mass Spectrometer

Chapter 3

Formic Acid, LC-MS Grade

Pierce Water, LC-MS Grade

3.4 Methods

As previously reported, modifications to an Orbitrap Elite (Thermo Scientific) including a Fusion™ reagent ion source allowed the front-end introduction of ETD reagent anion of 2,2′-biquinoline(15).

In these experiments, modifications were made also to the computer programs that run the instruments' embedded processors and control scanning of the mass spectrometer. These programs are written in a C-like proprietary programming language, ITCL; permissions were granted by ThermoFisher Scientific for modifications. These modifications allowed a single supplemental AC potential, dipolar broadband AC field, or both to be superposed on the RF quadrupolar trapping field for excitation of ions with resonant characteristic frequencies of motion in the quadrupole field during the ion/ion reaction.

One microliter of 1nmol/uL stock solution of ubiquitin was diluted with one milliliter of 40/60 acetonitrile/0.1% acetic acid in water. This solution was

infused directly to the instrument through a fused silica column equipped with a laser puller emitter at a rate of 100 uL/min.

Except where denoted, MS/MS parameters were as follows: low resolution mass analysis (normal scan rate) 500-2000 m/z, 1e4 precursor and 3e5 reagent AGC targets, 2 scans/spectrum, 5 m/z isolation window centered around 660 m/z, 50 ms ETD. For results presented in Figure 3.3, Orbitrap mass analysis was used with 3e5 reagent AGC at 60,000 resolution at 400 m/z.

3.5 Results

3.5.1 Single frequency parking during ion/ion reactions revealed large cation deviations from fundamental secular frequencies.

The focus of this dissertation chapter is to characterize ion motion during an ion/ion reaction. Alterations to ion motion due to mutual storage of large populations of anions and cations have not been previously characterized. This is primarily due to the nature of mass analyzers, which are not capable of simultaneous mass analysis of both ion polarities. Characterizing ion secular frequencies during the ion/ion reaction was accomplished indirectly by measuring changes in the ion/ion reaction rate (vide infra.)

Chapter 3

During the ion/ion reaction, a single supplemental AC potential was superposed onto the main RF quadrupolar trapping field. Ions with a secular frequency of motion in resonance with the supplemental AC potential are parked. Extensive ion/ion reaction times for highly charged species, i.e. 50 ms, should completely deplete the precursor when the ETD reactants are not parked. If the precursor remains after 50 ms of reaction time, then the precursor or reagent was parked by the supplemental AC potential. In other words, when there is precursor remaining after 50 ms of ETD reactions, the pseudo rate constant k′ for the ion/ion reaction is small; when the precursor is completely consumed after 50 ms, k′ is large. This experiment is repeated, each time changing the frequency of the supplemental AC potential. Overall, the supplemental AC frequencies at which the precursor was excited (low k′ values) reveals the precursor's secular frequency during the ETD reaction itself. In this fashion, it becomes possible for the first time to explore ion motion during the ion/ion reaction. This basic experiment, re-evaluated with various changing parameters such as anion and cation targets, comprises most of the experimental data presented in this chapter.

The initial experiment with this diagnostic is displayed in

Figure 3.1, using ubiquitin $[M+13H]^{13+}$ precursor ions at 660 m/z. It was hypothesized that due to self-space charging, the precursor would exist at a discrete band of frequencies just below its theoretical secular frequency of 111 kHz. However, it was surprisingly observed from this experiment that the precursor's actual secular frequencies are approximately 125-135 kHz during the ion/ion reaction, over 10% higher than the predicted secular frequencies. Secular frequencies of 125-135 kHz correspond to ions 590-635 m/z, deviating greatly from the precursor's 660 m/z.

The evaluation of effects due to changing the anion target on the precursor's secular frequencies was an illuminating experiment, as displayed in Figure 3.2. (An explanation of ion "targets" was provided in 1.4.4.) The larger the anion population, the more the precursor's secular frequencies shifted from the theoretical secular frequency. Therefore, the unexpected shift in precursor frequency was a result of simultaneous confinement of both ion polarities. It is speculated that at 1e5 reagent (when the reagent anion's Mathieu q_u is 0.7,) the anion cloud reached a sufficient degree of space charge to rival or exceed the RF trapping quadrupolar field of the LIT. In other words, the electric field created from the space charged anion cloud

contributes to the electric fields governing the cation is no longer exclusively defined by the ion trap's quadrupolar field. As a result, the cations

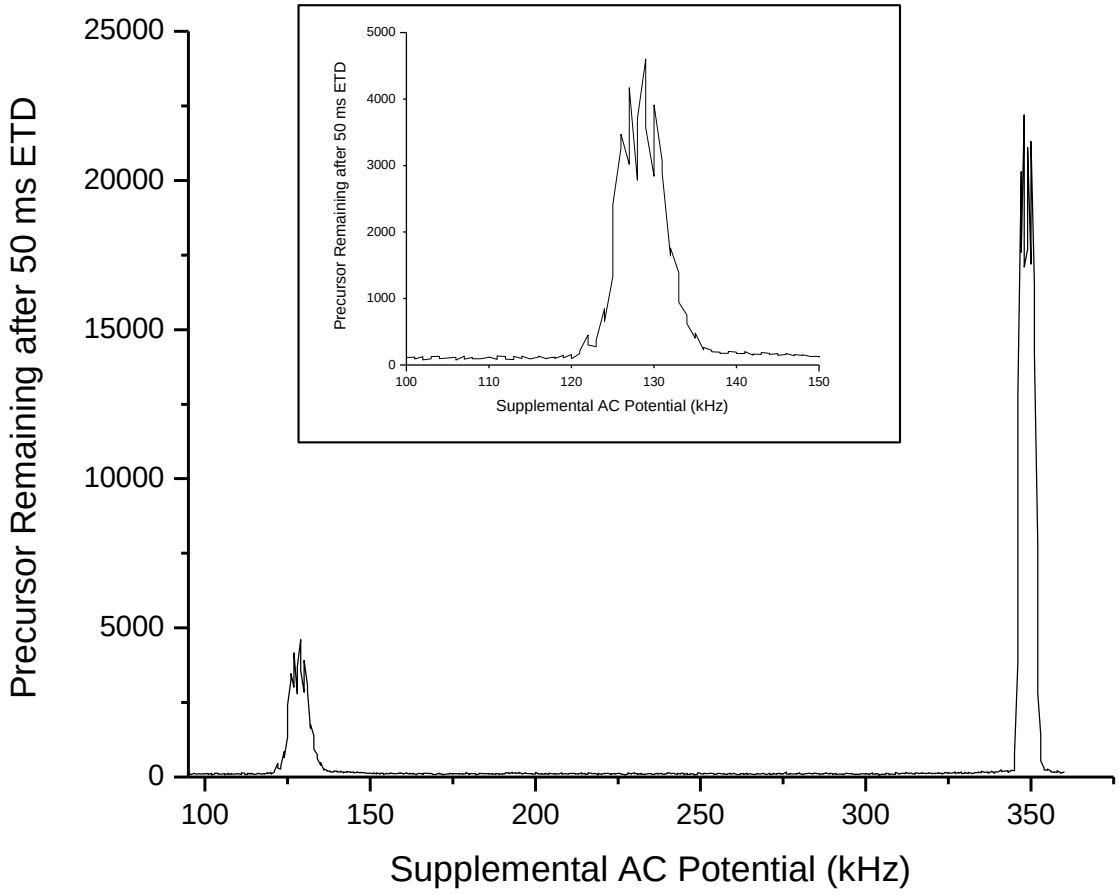

Figure 3.1 Single frequency parking of ubiquitin $[M+13H]^{+13}$. A single supplemental AC potential is used during the ETD reaction to determine the secular frequencies of the precursor. The theoretical secular frequency of ubiquitin $[M+13H]^{+13}$ precursor ion is 111 kHz; however, it is evident that under these ETD conditions, the precursor's actual secular frequencies are between approximately 125-135 kHz (inset). The secular frequencies of the 2,2'-biquinoline reagent anion are also observed centered around 350 kHz.

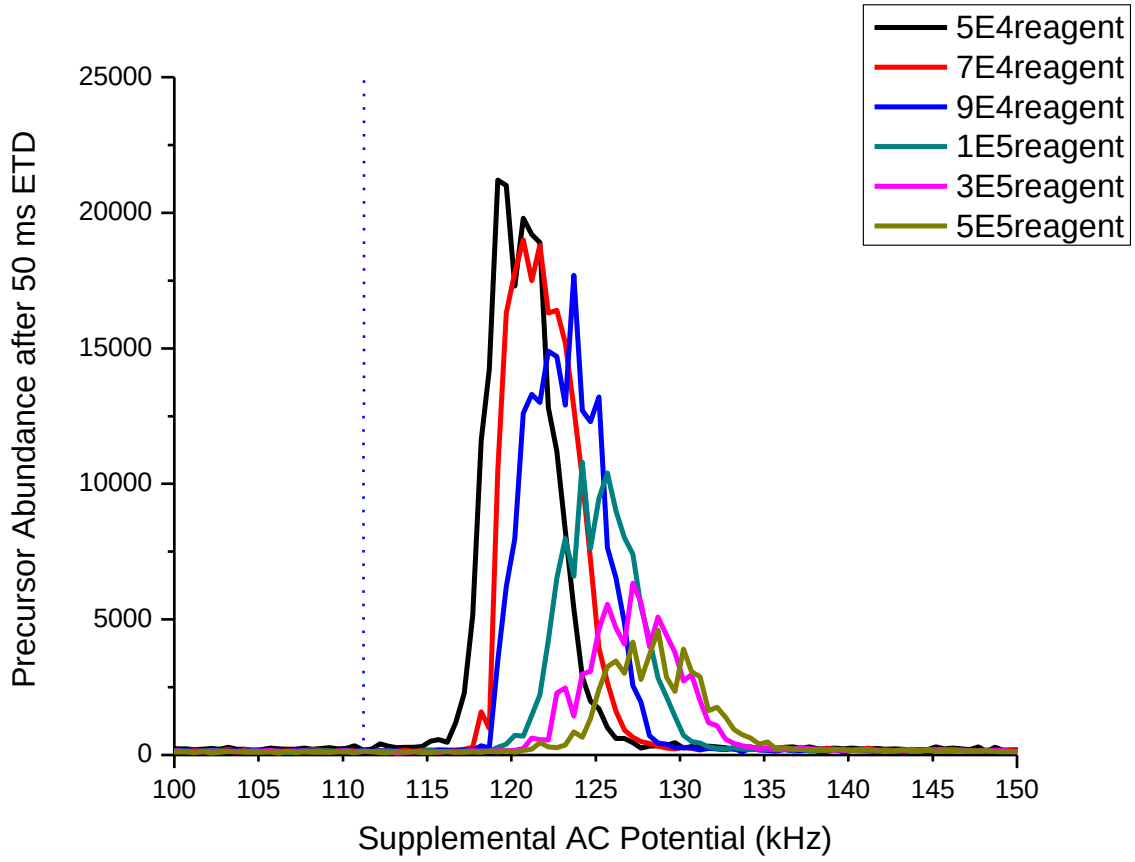

Figure 3.2. Single frequency parking of ubiquitin $[M+13H]^{+13}$ with varied reagent targets and constant 1E4 precursor. A single supplemental AC potential is used during the ETD reaction to determine the secular frequencies of the precursor as a function of reagent target. For these experiments, the precursor's theoretical secular frequency is 111 kHz (blue dashed line.)

deviate from their theoretical secular frequency with an inductive shift towards the anion frequency. It is predicted that the cations will approach the theoretical secular frequency of 111kHz as the reagent number is dropped below 5e4. These conditions were not evaluated as the ETD reaction rate drops precipitously with the reagent target, due to the lack of overlap

between the ion clouds as the anion cloud decreases its degree of self-space charging (3.2.2). The decrease in precursor abundance after 50 ms of reaction as reagent target increases-i.e. for 5e4 reagent the precursor abundance is 2e4, but it drops to 5e3 for 5e5 reagent- can also be correlated to the concomitant increase in ETD reaction rate.

Secular frequency of oscillation is an important descriptor of an ion in a quadrupolar electric field. This property must be known and predictable to stably trap and manipulate ions. Initially, this investigation aimed to show that the reacting species in an ion/ion reaction oscillated at many frequencies adjacent to the theoretical secular frequency, an expected phenomenon with space-charged ions in a quadrupolar field. An inductive shift in frequency between ion populations of opposite polarity simultaneously confined has not been previously observed. The large deviation from ideality and predicted secular frequencies under standard operating conditions was unexpected.

3.5.2 Characterizing deviations from fundamental secular frequencies

The anion's inductive effect on cations' secular frequencies varies with a number of operating parameters. Secular frequency is a defining characteristic of ions in a quadrupole ion trap; for any analytical purposes

involving resonant excitation during the ion/ion reaction (as will be discussed in Chapter 4 of this dissertation,) the secular frequency of the cations needs to be known. Otherwise, it is not possible to specifically resonantly excite ions. Therefore, the goal in this section of the dissertation is to explore conditions which minimize the cation frequency shift during ETD, in an endeavor to localize the cations' frequencies near the theoretical secular frequency. Mitigating the frequency shift was chosen as the route to creating predictable secular frequencies. Towards this goal, the effects of changing the number of cations and adding reagent kinetic excitation on the precursor's secular frequency during an ion/ion reaction were explored.

Although Figure 3.2 displays that large anion populations exacerbates an inductive shift on the cations' secular frequencies during ETD, the anion target remained 5e5 for these experiments. This was done to maintain predictable pseudo first order kinetics with the precursor for the ion/ion reaction, as well as to ensure there was sufficient reagent anion to react with all precursor cations.

3.5.3 Changes in the cation population can affect cations' secular frequency.

The affect the cation population size has on the anion-induced frequency shifts is demonstrated in Figure 3.3. The same experiment described in 3.5.1 with an auxiliary AC potential applied during an ion/ion reaction was employed with varying precursor targets of the $[M+13H]^{+13}$ of ubiquitin, and a constant reagent target of 5e5 anions. When the Mathieu q_u of the reagent anion was set to 0.70, the theoretical secular frequency of the precursor at 660 m/z is 111 kHz. Figure 3.3 reveals a trend that as the number of cations increase, the actual precursor frequencies shift closer to the predicted theoretical frequency at 111 kHz. Increasing the number of cations has a limited effect on the secular frequency shift of the cations; it is probable the cation will always have a secular frequency shifted high (*vide infra.)*

Based on these results, it can be reasoned that as the precursor population grows, the cation cloud is increasingly space charged, creating a combatting electric field to the electric field created by the space charged anions. Due to its tighter radial confinement in the ion trap, the degree of anion space charging will always exceed the cations' at these operating conditions. Therefore, the cations' frequencies will always be shifted slightly higher than theoretical. Note that at 1e5 and 3e5 precursor targets, which

are typical for high resolution mass analysis, the precursor's frequency range is adjacent to its theoretical secular frequency and spans roughly the same range for both targets. Therefore, precursor targets higher than 1e5 are desirable to localize the precursor's frequency of oscillation near its predicted secular frequency.

3.5.4 Resonant excitation of the reagent affects the cation frequencies.

Even though the ion populations are comparable, the strength of the electric field created from the low m/z anion cloud exceeds that of the high m/z cation cloud due to the anions' tighter spatial confinement in the oscillating quadrupole field (2, 16, 17). However, resonant excitation of an ion in this oscillating quadrupole field increases the ion's amplitude of oscillation in the LIT. It was hypothesized that such resonant excitation of the anion cloud would alleviate self-space charging and subsequently the inductive frequency shift imposed on the cation cloud.

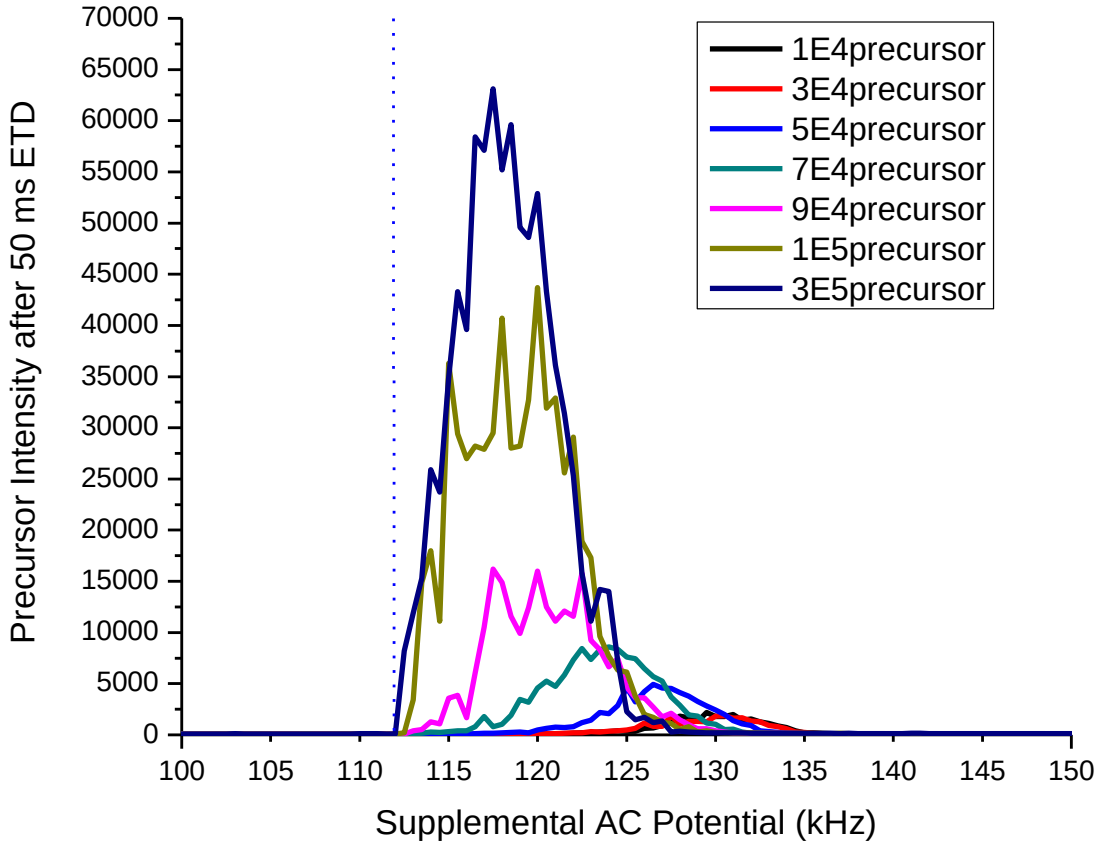

Figure 3.3. Single frequency parking of ubiquitin $[M+13H]^{+13}$ with varied precursor targets and 5E5 reagent target. A single supplemental AC potential is used during the ETD reaction to determine the secular frequencies of the precursor as a function of precursor target. For these experiments, the precursor's theoretical secular frequency is 111 kHz (blue dashed line.)

Figure 3.4 demonstrates the effects of resonant excitation of the anion cloud on the precursor's secular frequencies. At the lowest voltage of resonant excitation evaluated (2 mV), a definitive down shift of the precursor frequencies is observed. This trend continues as the voltage for resonant excitation is increased. At excitation voltages 4.5 mV and higher, the

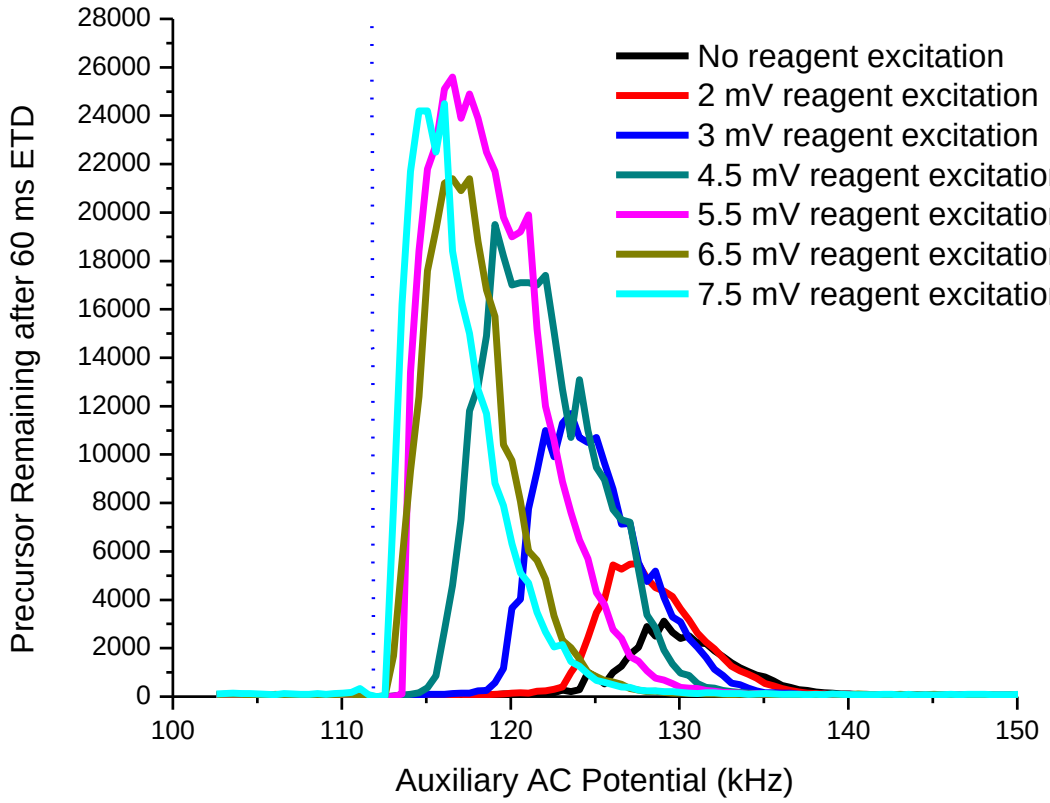

Figure 3.4 Single frequency parking of ubiquitin $[M+13H]^{+13}$ with 1E4 precursor ions and resonant excitation of the 5E5 reagent anions. A single supplemental AC potential is used during the ETD reaction to determine the secular frequencies of the precursor as the reagent anion cloud is resonantly kinetically excited. In these experiments, the theoretical secular frequency of the precursor is 111 kHz (blue dashed line.)

precursor frequencies are localized to just above its fundamental secular frequency. As the voltage for reagent excitation voltage is increases beyond 4.5 mV, the precursor cloud compacts even further but does not change its lowest frequency of oscillation in the ion trap. The increase in radial spread is proportional to the voltage of the resonant excitation potential, so the compaction of the precursor cloud is not entirely unexpected. Although

excitation of the reagent decreases the ion/ion reaction rate, the benefits of localizing the precursor's theoretical frequency near its predicted fundamental secular frequency was concluded to outweigh the detriment of decreased reaction rate.

3.6 Conclusions

The physics of ion motion during mutual storage in a quadrupolar ion trap of both ion polarities is not well-characterized. Presented here is a method to indirectly characterizing ion motion during the ion/ion reaction itself for the first time. Under typical ETD reaction conditions, it is shown that the electric field created by the anion cloud can rival the quadrupolar electric field of the LIT, so that cation motion is no longer solely defined by the quadrupolar field. Under these conditions, it is shown that cations do not retain their theoretical fundamental secular frequencies but adopt higher, unknown frequencies of oscillation in the LIT. This shift in secular frequencies can be mitigated by higher precursor targets and resonant excitation of the reagent.

3.7 References

1. March RE, Todd JFJ (2005) Quadrupole Ion Trap Mass Spectrometry (John Wiley & Sons, Inc). 2nd Ed. doi:10.1002/0471717983.
2. Tolmachev A V., Udseth HR, Smith RD (2000) Radial stratification of ions as a function of mass to charge ratio in collisional cooling radio frequency multipoles used as ion guides or ion traps. Rapid Commun Mass Spectrom 14(20):1907–1913.
3. Schwartz JC, Senko MW, Syka JEP (2002) A Two-Dimensional Quadrupole Ion Trap Mass Spectrometer. J Am Soc Mass Spectrom 13(02):659–669.
4. Todd JFJ, Waldren RM, Freer DA, Turner RB (2002) The quadrupole ion store (QUISTOR). Part X. Space charge and ion stability. B. On the theoretical distribution and density of stored charge in RF quadrupole fields. Int J Mass Spectrom Ion Phys 35(1–2):107–150.
5. Guan S, Marshall AG (1994) Equilibrium space charge distribution in a quadrupole ion trap. J Am Soc Mass Spectrom 5(2):64–71.
6. Qiao H, Gao C, Mao D, Konenkov N, Douglas DJ (2011) Space-charge effects with mass-selective axial ejection from a linear quadrupole ion trap. Rapid Commun Mass Spectrom 25(23):3509–3520.
7. Guo D, et al. (2014) Space charge induced nonlinear effects in Quadrupole ion traps. J Am Soc Mass Spectrom 25(3):498–508.
8. Cox KA, Cleven CD, Cooks RG (1995) Mass shifts and local space charge effects observed in the quadrupole ion trap at higher resolution. Int J Mass Spectrom Ion Process 144(1–2):47–65.
9. Mandal P, Das S, De Munshi D, Dutta T, Mukherjee M (2014) Space charge and collective oscillation of ion cloud in a linear Paul trap. Int J Mass Spectrom 364(1):16–20.
10. Mather RE, Todd JFJ (1980) The quadrupole ion store (QUISTOR). Part

VII. Simultaneous positive/negative ion mass spectrometry. Int J Mass Spectrom Ion Phys 33:159.

11. Williams JD, Cooks RG (1993) Reduction of Space-charging in the Quadrupole Ion Trap by Sequential Injection and Simultaneous Storage of Positively and Negatively Charged Ions. 7(March):380–382.
12. Stephenson JL, McLuckey SA (1997) Anion Effects on Storage and Resonance Ejection of. Anal Chem 69:3760–3766.
13. Syka JEP, Coon JJ, Schroeder MJ, Shabanowitz J, Hunt DF (2004) Peptide and protein sequence analysis by electron transfer dissociation mass spectrometry. Proc Natl Acad Sci 101(26):9528–9533.
14. Compton PD, Strukl J V., Bai DL, Shabanowitz J, Hunt DF (2012) Optimization of electron transfer dissociation via informed selection of reagents and operating parameters. Anal Chem 84(3):1781–1785.
15. Earley L, et al. (2013) Front-end electron transfer dissociation: A new ionization source. Anal Chem 85(17):8385–8390.
16. Xia Y, Wu J, McLuckey SA, Londry FA, Hager JW (2005) Mutual storage mode ion/ion reactions in a hybrid linear ion trap. J Am Soc Mass Spectrom 16(1):71–81.
17. Zhang X, et al. (2016) Reducing Space Charge Effects in a Linear Ion Trap by Rhombic Ion Excitation and Ejection. J Am Soc Mass Spectrom 27(7):1256–1262.

Chapter 4

4. Development of Parallel Ion Parking During ETD to Improve Conversion of Parents to First-Generation Products

4.1 Overview

Electron transfer dissociation (ETD) is an analytically useful tool for primary structure interrogation of intact proteins, but its utility can be limited by sequential reactions of the products. For a method known as parallel ion parking during ETD (PIP-ETD), a tailored waveform is applied during ETD to resonantly kinetically excite the first-generation ETD products, inhibiting higher order product formation. Experimental optimization is used determine sufficient waveform amplitudes and frequency exclusions for the precursor ion, making PIP-ETD user friendly. Analysis with PIP-ETD of standard proteins (8 kDa ubiquitin, 17 kDa apomyglobin, 20 kDa human histone H1, and 21 kDa Protein G) returns high rates of complementary fragment ions, demonstrating preservation of first generation ETD products.

Chapter 4

4.2 Introduction

4.2.1 Challenges of ETD Interrogation of Intact Proteins

To be useful in determining the primary structure of a peptide or protein by MS/MS, a fragment product ion must have the N- or C-terminus of the parent precursor cation. A single ETD reaction of the precursor will ideally produce 2 first-generation ETD fragments, each possessing a termini of the precursor (Figure 4.1). Sequential ETD events will produce higher generation

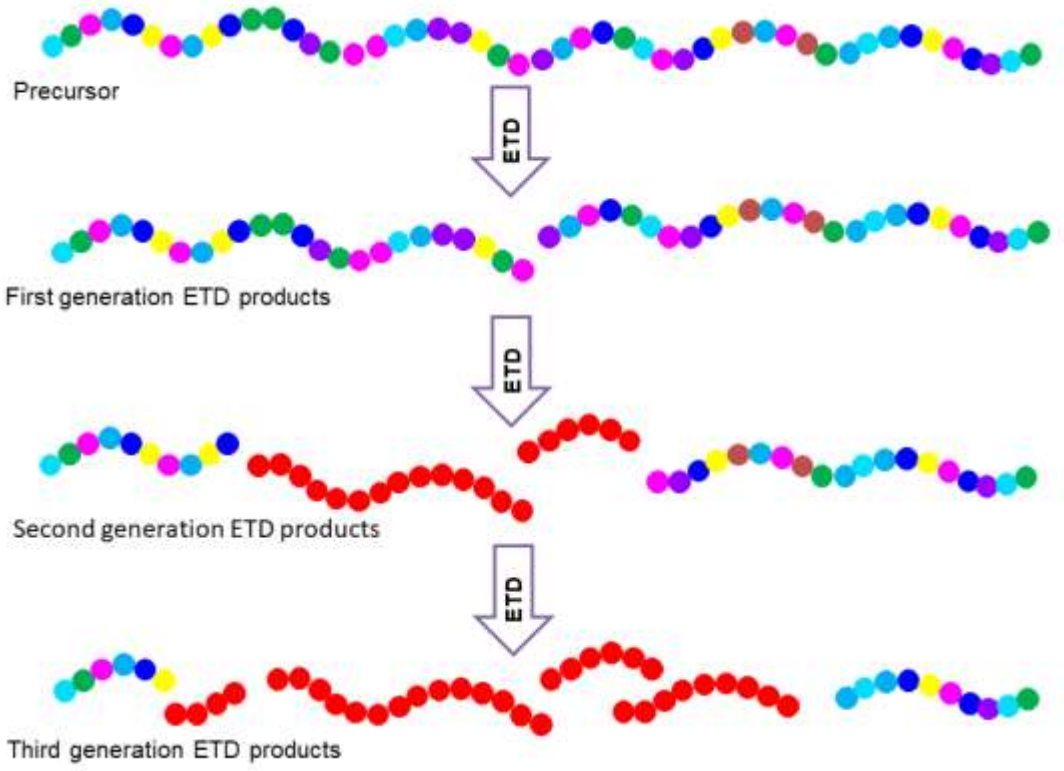

Figure 4.1. A single ETD reaction of the precursor ion will form two first generation ETD fragments. Subsequent ETD reactions will produce internal fragments (red) and increasingly smaller ions containing the protein termini (multicolor.)

fragments, creating "internal fragments" that do not possess one of the precursors' termini. Sequential reactions are undesirable because they decrease the overall signal for informative fragment ions and complicate the spectrum with internal fragment ions.

Electrospray ionization of intact proteins produces highly charged cations; since a single ETD reaction will neutralize only one charge, the first-generation ETD fragments will also be highly charged. Recall ion/ion reaction rates have the following relationship:

$$k \propto v\left(\frac{Z_1^2 Z_2^2 e^4}{\varepsilon_0 (\mu v^2)^2}\right) \qquad (4.1)$$

in which Z1 and Z2 are the charges of the reactants, e is the elementary charge, ε_0 is the vacuum permittivity, μ is the reduced mass, and v is the relative velocity between the reacting species. Specifically, Equation 4.1 demonstrates that ion/ion reaction rates can be heavily influenced by the charges on the reacting species. When both precursor and product ions have similarly high charge states, the insignificantly different reaction rates lead to similar production rates of first- and higher-order generation products. To avoid internal fragmentation, the ETD reaction is stopped before the precursor is completely consumed. The point of minimal secondary product ions and

maximum efficiency is when significant amounts of the precursor ion are unreacted. For peptides with 2 or 3 charges, the maximum efficiency is when one half to two thirds of the precursor population remains; less of the precursor is consumed at maximum efficiency as the precursor grows in charge (1, 2). Unfortunately, since intact proteins have many dissociation channels, it is even more desirable to fragment as much of the precursor population as possible to increase fragment ion signal. A method to increase differential ETD reaction rates between precursor and product ions would be useful for intact protein interrogation by ETD MS/MS.

4.2.2 Parallel ion parking during ETD

A method of inhibiting sequential ETD fragmentation in quadrupole ion traps was developed by Chrisman et al. and demonstrated on peptides (3). Recall that in the technique known as ion parking, a single AC potential is used to kinetically excite a single ion with a resonant secular frequency, decreasing that ion's reaction rate. In the method "parallel ion parking" or PIP, a tailored waveform composed of many AC potentials is superposed onto the RF trapping field during the ETD reaction to resonantly kinetically excite only first-generation ETD products. In this way, the first-generation ETD products are prevented from further fragmentation. No frequencies corresponding to

the precursor ion are incorporated into the PIP-ETD waveform, allowing the precursor to react at an uninhibited reaction rate (i.e. the precursor reacts very quickly.) This creates a large difference between the reaction rate of the precursor and secondary ETD products, allowing for greater consumption of the precursor without formation of internal fragments. With PIP-ETD, Chrisman et al. demonstrated greater than 90% of the precursor was converted to first generation ETD product ions.

4.2.3 Current Limitations to PIP-ETD

Although the initial work of Chrisman et al. demonstrated that PIP-ETD preserved most first-generation fragments for peptides, the goal of the research presented in this chapter of the dissertation was to extend the methodology to intact proteins. This endeavor was complicated by the desire to park all the ETD product ions and choosing an appropriate voltage for each frequency in the PIP-ETD waveform.

The first adaptation from PIP-ETD as presented by Chrisman et al. was the inclusion of high frequencies in the waveform to park all ETD product ions. Chrisman et al. report a 50% increase in first generation ETD product ions but there were no components in the waveform to park product ions with secular frequencies higher than the precursor. That exclusion in the

waveform left a subpopulation of the sequence-informative ions unpreserved. This subpopulation will grow with the size of the precursor, limiting the method's use for intact proteins. While theoretically the PIP-ETD waveform could include frequencies higher than the precursor, initial investigations incorporating higher frequencies resulted in a dramatically lower precursor reaction rate. This is presumably due to inadvertent kinetic excitation of the precursor, as Chapter 3 of this dissertation explains that the precursor's secular frequency is shifted during an ion/ion reaction. The variance of precursor secular frequencies during an ion/ion reaction is a complex phenomenon dependent on many experimental variables, such as ion populations and Mathieu q_u's of the ions. To park ETD fragment ions with secular frequencies higher than the precursor, the precursor's secular frequencies need to be well-defined for the reaction conditions.

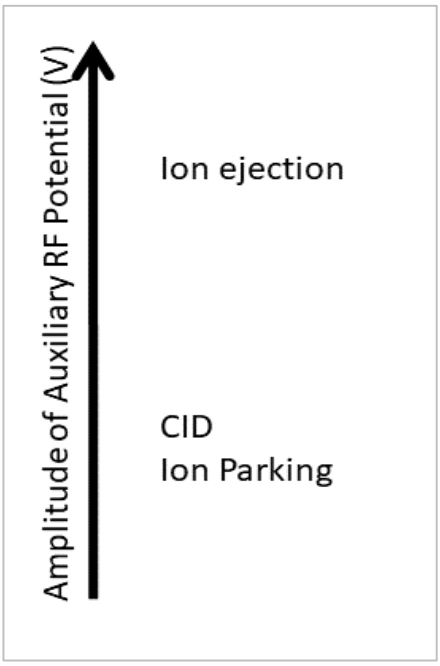

Figure 4.2. Effects of PIP-ETD waveform amplitude on resonant ion.

The second obstacle to applying PIP-ETD to interrogate intact proteins is choosing the correct voltage for each frequency in the waveform. Slight resonant excitation will increase an ion's average velocity in the LIT and decrease its ion/ion reaction rate, the ideal voltage for ion parking. Excess excitation could result in two undesirable phenomena: collisional induced dissociation (CID) or ejection from the LIT, as depicted in Figure 4.2. It is possible that through resonant kinetic excitation the ion will accelerate sufficiently that collisions with the bath gas in the LIT will fragment the ion. Too much resonant excitation could also accelerate the ion such that it develops an unstable trajectory in the quadrupolar field and is ejected from the LIT.

Since ions at different frequencies resonantly absorb power from the auxiliary waveform with different efficiencies, each AC component comprising the waveform needs a different voltage, or amplitude (4–6). High frequency ions resonantly absorb power from the waveform with greater efficiency,

therefore the waveform AC components for higher frequency ions need lower amplitudes. Conversely, low frequency ions resonantly absorb power with less efficiently, and the waveform AC components corresponding to these ions need higher amplitudes. To date, ion parking methods have experimentally optimized the auxiliary AC amplitudes. Scott McLuckey's original work with ion parking empirically determined sufficient voltages for the auxiliary AC potential to not fragment or eject the ions, as did the original PIP-ETD work by Chrisman et al. (3, 7). When integrating ion parking with UVPD, Holden et al. used time-intensive experiments to determine the ideal frequency and sufficient amplitude for ion parking (8). In the analysis of intact histone proteins, the amplitude of the waveform used for PIP-IIPT by Anderson et al. was experimentally determined (9). In each of these studies using ion parking, the ideal voltages were experimentally determined for specific precursors. Characterizing ideal voltages for each frequency in a PIP-ETD waveform so that the waveform is robust and applicable to any precursor has not been attempted.

Presented in this chapter is analytically useful routines to optimize PIP-ETD conditions and results from PIP-ETD applications. First, appropriate voltages/amplitudes for each AC potential in the PIP-ETD waveform are

characterized. The second optimization is to determine the exact secular frequencies of various precursors; these frequencies are ultimately excluded in the waveform so as not adversely affect precursor reaction rates. The resulting waveform is used to evaluate sequence coverage of several standard intact proteins.

It is relevant to note that these optimizations rely on constant ion targets and are only applicable to the ion targets used to optimize. Additionally, results are presented in terms of the ion's Mathieu q_u identity. For clarity, this property directly correlates with the ion's secular frequency.

4.3 Materials, Equipment, and Instrumentation

Honeywell (Morristown, NJ)

Burdick and Jackson Acetonitrile, LC-MS grade

Millipore (Billerica, MA)

Amicon® Ultra-0.5 10K centrifugal filter

Molex (Lisle, IL)

Polymicro Technologies™ polyimide coated fused silica capillary, 360 µm o.d. x 75 µm i.d.

New England Biolabs (Ipswich, MA)

Histone H1, Human Recombinant

Chapter 4

Oakwood Chemical (Estill, SC)

Perfluoromethyldecalin

Sigma Aldrich (St. Louis, MO)

2,2′-biquinoline, >99% purity

Apomyoglobin from equine skeletal muscle,

protein sequencing standard, lyophilized powder

Ubiquitin from bovine erythrocytes

Sutter Instrument Co. (Navato, CA)

P-2000 microcapillary laser puller

Tektronix (Beaverton, OR)

MDO3014 Mixed domain oscilloscope

ThermoFisher Scientific (San Jose, CA; Bremen, Germany)

Orbitrap™ Elite Hybrid Ion Trap-Orbitrap Mass Spectrometer

Pierce Water, LC-MS Grade

Pierce Protein G, Recombinant lyophilized powder

Chapter 4

Methods

4.3.1 Sample preparation

One microliter of 1nmol/uL stock solution of ubiquitin was diluted with one milliliter of 40/60 acetonitrile/0.1% acetic acid in water. One microliter of 1nmol/uL stock solution of apomyoglobin was diluted with one milliliter of 40/60 acetonitrile/0.1% acetic acid in water.

Five milligrams of powdered Protein G were reconstituted with 1 milliliter of water. Four microliters of this stock solution was diluted to one milliliter with 40/60 acetonitrile/0.1% acetic acid in water for an approximate final concentration of 1 pmol/uL.

Twenty-five microliters of the 1mg/mL Histone H1 solution was diluted to 1 milliliter with 40/60 acetonitrile/0.1% acetic acid in water for an approximate final concentration of 1 pmol/uL.

These solutions were infused directly to the instrument through a fused silica column equipped with a laser puller emitter at a rate of 100 uL/min.

4.3.2 Instrument and Software modifications

As previously reported, modifications to an Orbitrap Elite (ThermoFisher Scientific) including a Fusion^{TM} reagent ion source allowed the front-end

introduction of ETD and IIPT reagent anions, from 2,2′-biquinoline and perfluoromethyldecalin respectively. The introduction of reagent ions through the front of the instrument allowed products from multiple iterations of ion/ion reaction products to be accumulated in the C-trap prior to a single Orbitrap high-resolution mass analysis.

In these experiments, modifications were made also the computer programs that run the instruments' embedded processors and control scanning of the mass spectrometer. These programs are written in a C-like proprietary programming language, ITCL; permissions were granted by ThermoFisher Scientific for modifications. These modifications allowed a single supplemental AC potential, waveforms, or both to be superposed on the RF quadrupolar trapping field for excitation of ions with resonant characteristic frequencies of motion in the quadrupole field during the ion/ion reaction. Frequencies and amplitudes comprising the waveforms are described in the following section for each experiment.

4.3.3 Calibration of waveform amplitude as a function of precursor q_u

For these experiments, the $[M+13H]^{13+}$ of ubiquitin was employed as the precursor ion. The RF trapping voltage was adjusted to correspond to a Mathieu q_u of 0.400, 0.450, 0.500, 0.550, 0.600, 0.650, 0.700 and 0.750 relative

to the 2,2'-biquinoline reagent anion, placing the precursor at Mathieu q's of 0.155, 0.175, 0.194, 0.213, 0.233, 0.252, 0.272, and 0.291 respectively. For all these experiments, the reagent anion is resonantly excited with a broadband 0.5mV AC field centered at the reagent's fundamental secular frequency.

A waveform with 26 AC potential components spanning 37.5 kHz in 500 Hz increments, centered around the precursor ion's fundamental secular frequency, is applied during 40 ms of ETD. The amplitude of this waveform is incrementally increased. Two metrics were plotted at each amplitude. First, the intensity of 726 m/z, z=+4 fragment ion of ubiquitin that manifests prominently during collisional dissociation, is recorded. Second, the total ion current before and after the 40 ms of parked ETD is also recorded to evaluate if there is ion ejection during ETD parking. The ion current remaining after 40 ms parked ETD is evaluated as:

$$remaining\ ion\ current\ after\ 40\ ms\ parked\ ETD = \frac{TIC\ after\ 40\ ms\ ETD}{TIC\ before\ 40\ ms\ ETD} * 100 \quad (3.2)$$

Where "TIC" denotes total ion current. Ideal amplitudes for the parking waveform were evaluated as a function of the precursor's Mathieu q. At each Mathieu q_u, two waveform amplitudes were evaluated: the amplitude at which the collisional fragment at 726 m/z exceeded 6e3 intensity and the amplitude at which less than 80% of the ion current remained after 40 ms

ETD (ejection amplitude). These threshold values were designated as approximate points where resonant excitation had severe effects on the cations. If the amplitude for collisional dissociation was lower, that amplitude was assigned as the ideal parking waveform amplitude for that Mathieu q_u of the precursor. If the ejection amplitude was lower of the two, that amplitude was reduced by 10% and assigned as the ideal parking amplitude for that Mathieu q_u.

Once ideal parking amplitudes for each precursor Mathieu q_u were selected, the waveform was created as a function of the precursor q_u. Since the same m/z ion was used to determine these amplitudes, it was necessary to correct the amplitudes so that equivalent forces would be exerted on different size ions. This was done after fixing the reagent's (2,2′-biquinoline) Mathieu q_u at 0.8:

$$A_{new} = \frac{A_{Ubi\ 13H}(m/z)_{new}}{660\ m/z} \qquad (3.3)$$

Where A_{new} is the new amplitude, $A_{Ubi\ 13H}$ is the calibrated amplitude for ubiquitin $[M+13H]^{+13}$ precursor as determined vide infra, $(m/z)_{new}$ is the m/z of the ion at ubiquitin $[M+13H]^{+13}$'s Mathieu q_u during calibration when the reagent's Mathieu q_u is fixed at 0.80, and 660 m/z describes the ubiquitin $[M+13H]^{13+}$ ion.

MS/MS parameters were as follows: Orbitrap mass analysis from 500-2000 m/z, 3e5 reagent AGC target, 1e5 precursor AGC target, r=120,000 at 400 m/z, one scan/spectrum.

4.3.4 Calibration of precursor notch widths in the waveform

For these experiments, the $[M+13H]^{13+}$, $[M+12H]^{12+}$, $[M+11H]^{11+}$, $[M+10H]^{10+}$, $[M+9H]^{9+}$, and $[M+8H]^{8+}$ charge states of ubiquitin were evaluated as the precursor ions while the Mathieu q_u was fixed at 0.80 relative to the reagent anion.

A waveform consisting of 26 frequencies in 500 Hz increments was applied during ETD. These waveforms placed the frequencies starting at 80 kHz and shifted the frequencies up 500 Hz at time, until the starting frequency in the waveform was at 160 kHz. The reaction rate of the precursor for each reaction as the waveform shifted was evaluated by measuring the abundance of the precursor ion remaining after 150 ms ETD. The amplitude of the AC potentials comprising the waveform were set by frequency as determined in 4.3.3.

The MS/MS parameters were as follows: Orbitrap mass analysis from 500-2000 m/z, 3e5 reagent AGC target, 1e5 precursor AGC target, r=120,000 at 400 m/z, one scan/spectrum.

4.3.5 Performance evaluations

For the results presented in Figure 9, MS/MS parameters were as follows: the various charge states of apomyoglobin were isolated with a 5 m/z window, 1e5 precursor and 3e5 reagent AGC targets in ion trap mass analysis (normal scan rate,) 2 scans/spectrum. Three repeat measurements were averaged per data point.

For sequence coverage analysis of ubiquitin, apomyoglobin, histone H1, and Protein G, each solution was infused per section 4.3.1. Orbitrap MS/MS parameters were as follows: 3e5 reagent and 1e5 precursor AGC, 5 m/z isolation window of the precursor, 500-3500 m/z scan range, 7 multiple fills of the product ions into the C-trap, and 16 scans/spectrum, r=120,000 at 400 m/z. The MS/MS spectra were examined using Qual Browser software (ThermoFisher Scientific). Interpretation of the ETD/IIPT MS/MS was performed manually on the unprocessed raw spectra, averaging 25-35 MS/MS spectra. Percent sequence coverage was calculated by dividing the number of the observed N-Cα bond cleavages by the total numbers of predicted N-Cα bond cleavages. Although cleavage of the N-Cα bond that is N-terminal to proline does not produce an observable fragment, it is counted as a missed cleavage to not artificially inflate sequence coverage. Masses for all intact

fragments identified were within 5 ppm of the predicted masses, as calculated by an in-house fragment mass calculator.

4.4 Results and Discussion

4.4.1 Calibration of PIP-ETD waveform amplitude as a function of precursor q

Ubiquitin was chosen as the model protein for these experiments for three reasons. First, at 8.5 kDa, it is the smallest protein for which ETD parking is useful. Larger proteins require more vibrational excitation from collisions with the bath gas for fragmentation; calibrating amplitudes for a PIP-ETD parking waveform with a small protein ensures that larger proteins will be resonantly excited but not fragmented. Second, ubiquitin produces a prominent fragment from excessive collisions with the bath gas. This fragment is from dissociation of the peptide backbone at a proline residue (P19), the most fragile bond for vibrational excitation in the peptide backbone. This particular, abundant fragment ion (y_{58}^{+9}) is therefore monitored in these experiments to evaluate to what extent the PIP-ETD waveform causes CID of the precursor. Third, using the same precursor for these experiments, the $[M+13H]^{13+}$ of ubiquitin, ensures a uniform threshold energy for dissociation at various conditions.

The PIP-ETD waveform amplitudes were optimized first. Ions can be excited off-resonance, in which an adjacent frequency to an ion's secular frequency can slightly excite said ion. This affect is exacerbated the higher amplitude of the adjacent frequency. Thus, it was decided to optimize the amplitudes of the PIP-ETD waveform components first and use these amplitudes for the remainder of the optimization for consistency.

Figure 4.3 displays the results of increasing waveform amplitude on collisional fragmentation (Figure 4.3A) and ejection of the precursor ion (Figure 4.3B) after 40 ms parked ETD for Ubiquitin $[M+13H]^{13+}$ when the reagent Mathieu q_u was 0.75. Since CID and ion ejection from the LIT indicate excessive kinetic excitation, the ideal parking amplitude for precursors at those Mathieu q_u values is lower than an amplitude that ejects or fragments the precursor. The minimal amplitude for CID was defined by production of 6e3 signal intensity of the monitored fragment ion. The minimal amplitude for ejection was defined as the amplitude that retained less than 80% of the initial ion current. These minimal amplitudes are seen in Figure 4.4 as a function of precursor's Mathieu q_u.

Ions with a low Mathieu q_u value were found to be ejected from the LIT before collisional fragmentation occurred. With no or negligible DC offsets/a_u

parameter, ions are stably trapped in perfectly quadrupolar electric field when they possess a Mathieu q_u identity between 0 and 0.908. As the ion's Mathieu q_u approaches either of these boundaries, its confinement in the ion trap becomes less stable. Additionally, the electric field created by the LIT is not perfectly quadrupolar. Higher order resonances and nonlinearities in the electric field do exist, particularly when the ion is closer to the electrode surface as is characteristic of low Mathieu q_u ions. Although this has not been previously reported, it is not surprising that ions at lower Mathieu q_u's (Mathieu q_u < 0.2 in Figure 4.4) develop unstable trajectories in the LIT when resonantly kinetically excited and are ejected from the LIT.

The waveform amplitude at which the collisional fragment formed was used as the maximum amplitude for a parking waveform. Unlike during PIP-ETD, the precursor in these experiments is being directly excited and more likely to fragment from CID, so it was deemed not necessary to reduce these experimentally determined waveform amplitudes for PIP-ETD purposes. For ions with a low Mathieu q_u identity such that ion ejection is observed before CID, an amplitude 10% less than the ejection amplitude was used. These amplitudes were plotted as function of the precursor's Mathieu q_u (which

corresponds to specific AC frequencies,) and intervening frequencies were assigned amplitudes by extrapolating between the experimental data points.

The resulting PIP-ETD waveform for a standard protein used for MS/MS analysis, 17 kDa apomyoglobin $[M+26H]^{+26}$ precursor, is seen in Figure 4.5. Two things are noteworthy in Figure 4.5: that only products ions with frequencies lower than 210 kHz are parked and the inclusion of frequency components around 400 kHz. At these conditions, it is unlikely product ions will have frequencies higher than 200 kHz, so it was deemed unnecessary to include those frequency components. The flat amplitude frequency components centered around 400 kHz are used for resonant excitation of the reagent, per 3.5.4.

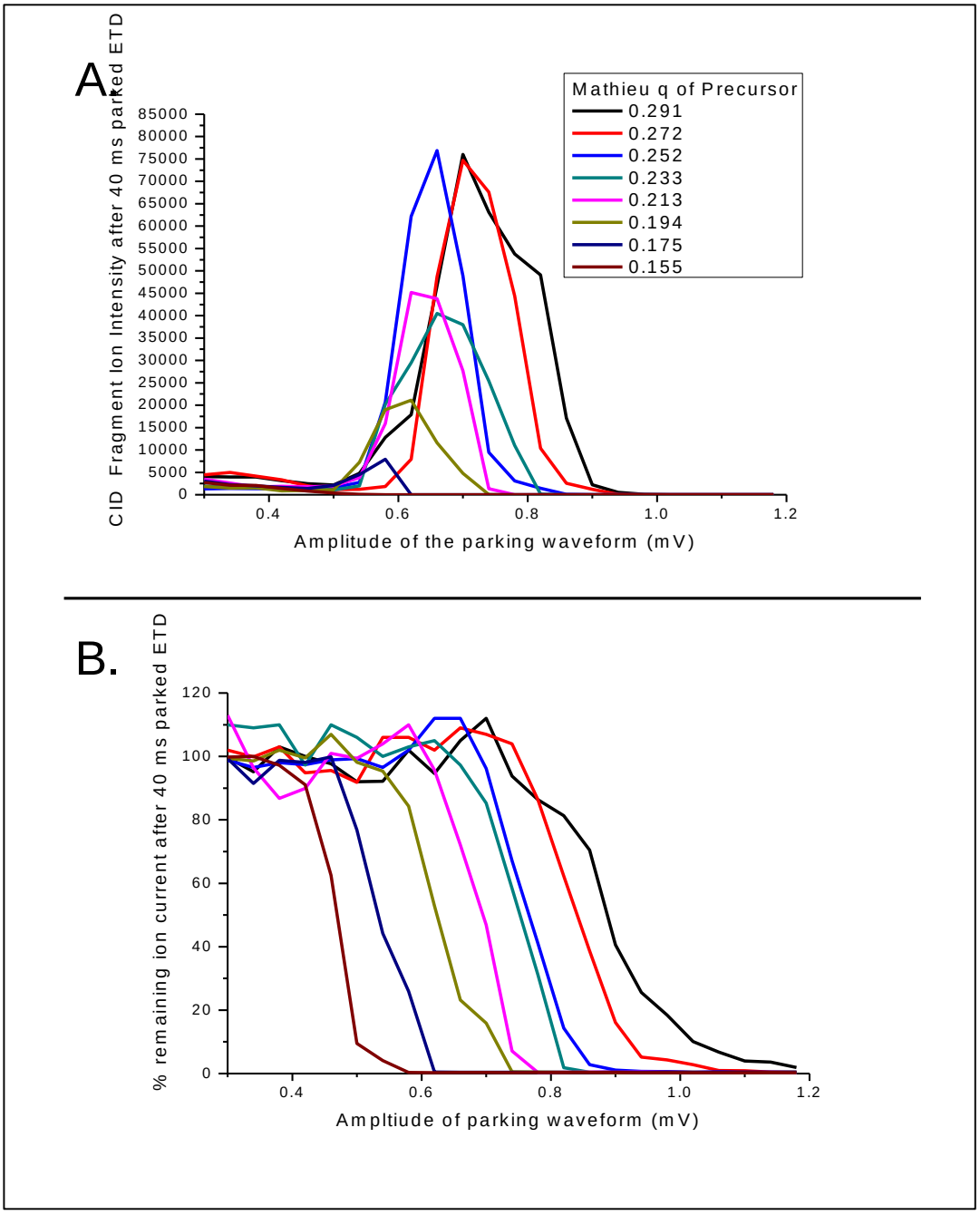

Figure 4.3. To evaluate the amplitude of the PIP-ETD waveform necessary to collisional dissociate (A) or eject (B) the ubiquitin $[M+13H]^{13+}$ precursor, the amplitude of the PIP-ETD waveform was incrementally increased. A) The intensity of a prominent CID fragment of ubiquitin, y_{58}^{+4}, is monitored to identify the PIP-ETD waveform amplitude that causes CID. B) The total ion current before and after PIP-ETD is monitored to identify the waveform amplitude at which ions are ejected from the LIT.

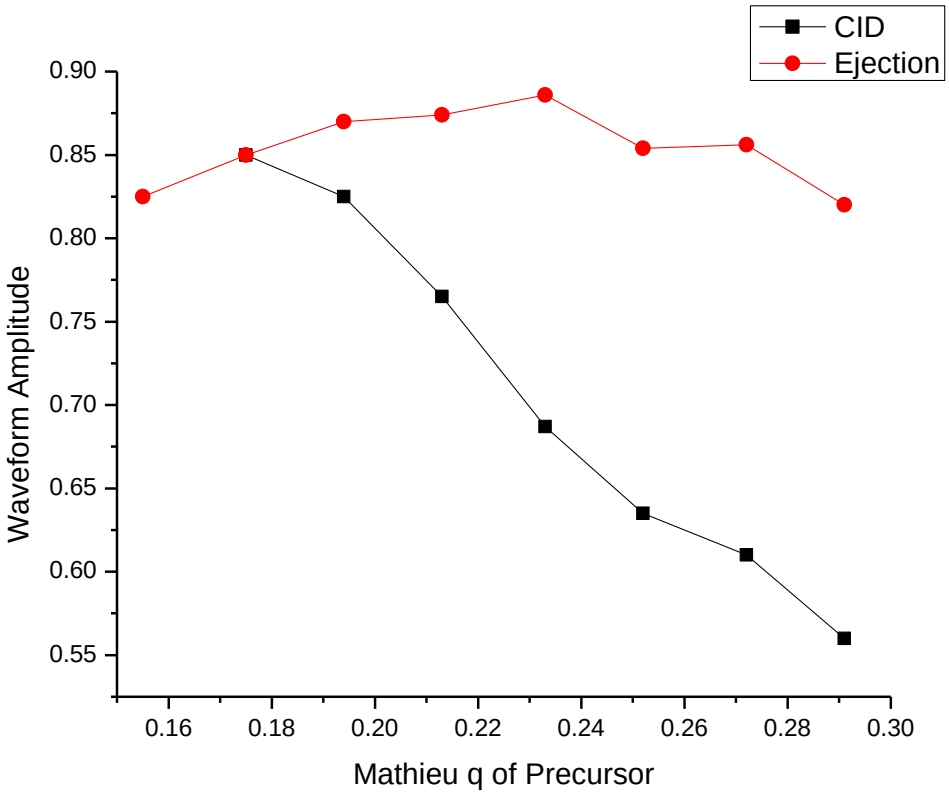

Figure 4.4. From the data in Figure 1, the minimal amplitudes of the PIP-ETD waveform necessary to eject and cause CID of ubiquitin $[M+13H]^{13+}$ precursor are displayed as a function of the precursor's Mathieu q.

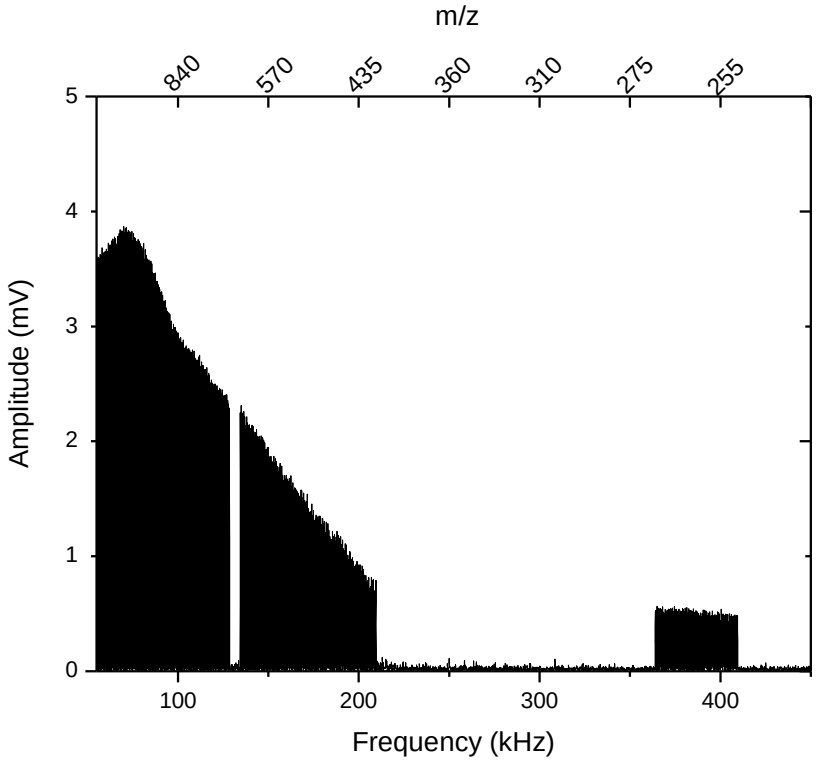

Figure 4.5. The PIP-ETD waveform to park 17 kDa apomyoglobin $[M+26H]^{+26}$ at 653 m/z, with the amplitudes and precursor notch width as calibrated in 4.4.1 and 4.4.2.

4.4.2 Calibration of precursor notch widths in the waveform

The PIP-ETD waveform needs to exclude frequencies corresponding to the precursor ion, creating a "precursor notch." If the precursor is resonantly kinetically excited, the reaction rate of the desired reaction is dramatically reduced. As explained in Chapter 3 of this dissertation, the precursor in an ion/ion reaction not only adopts more frequencies than its single theoretical

frequency, but those frequencies can differ significantly from the theoretical frequency.

The frequency dispersion between m/z values decreases as ion increases in m/z. This means a lower m/z precursor will occupy fewer shifter, secular frequencies than a higher m/z precursor. Thus, it is necessary to determine a precursor's secular frequencies with several different precursors of different m/z values.

Since the precursor's secular frequencies are altered by a number of operating parameters (i.e. voltage of resonant excitation potentials for the reagent, the reagent's Mathieu q_u, and ion targets), it is necessary that these parameters remain constant.

To determine the precursor frequencies to exclude in the precursor notch of the PIP-ETD waveform, a large waveform of 28 AC potentials in 500 Hz increments (spanning a total of 14 kHz) was applied during ETD with a fixed 1e5 precursor target and 5e5 reagent target at a Mathieu q_u of 0.80. The waveform was initially placed between 80-94 kHz, then the effect on precursor reaction rate was evaluated by precursor depletion after 150 ms ETD. The waveform was then moved to 81.5-94.5 kHz, and the effect on precursor reaction was again evaluated. This process was repeated, shifting

the waveform 500 Hz at a time until the final waveform spanned 146-160 kHz. The amount of precursor remaining was plotted as a function of the highest and lowest frequency component of each waveform. The results of this experiment with ubiquitin [M+13H]+13 can be seen in Figure 4.6.

A cutoff of 2e4 precursor remaining after 150 ms ETD was defined as the point where the applied waveform had too great an effect on the precursor reaction rate. In Figure 4.6, we can see that when the waveform is applied closer than about 1 kHz below or 5.5 kHz above the precursor's theoretical secular frequency of 128.6 kHz, the precursor reaction rate starts to be slowed. For a precursor at this Mathieu q, it was concluded that the precursor notch in the PIP-ETD waveform needs to be 6.5 kHz wide, excluding frequencies between 1 kHz lower and 5.5 kHz higher than the precursor's theoretical secular frequency.

This evaluation for determining the notch widths were repeated using the $[M+12H]^{12+}$, $[M+11H]^{11+}$, $[M+10H]^{10+}$, $[M+9H]^{9+}$, and $[M+8H]^{8+}$ at 715 m/z, 779 m/z, 857 m/z, 953 m/z, and 1071 m/z, respectively, as the precursor. It is unlikely to find precursors with m/z values lower than 600 m/z. It has also been shown that precursors with charge density less than 1000 m/z are less likely to fragment from an ETD reaction (11). Therefore, these precursors

span the m/z range in which a precursor for ETD is likely to be selected. The resulting determinations for necessary precursor notch widths are shown in Figure 4.7. Figure 4.7 demonstrates that while the notch for frequencies lower than the precursor remains mostly independent of the precursor's identity, the necessary notch width for higher frequencies than the precursor varies almost linearly with the precursor's Mathieu q_u. The necessary precursor notch widths were programmed to be calculated as a function of the precursors' Mathieu q_u. Precursors with Mathieu q_u identities not determined here were assigned notch widths by interpolating between experimental data points in Figure 4.7.

4.4.3 Performance evaluations of the PIP-ETD waveform

The calibrations for waveform amplitudes in section 4.4.1 and the precursor notch widths in section 4.4.2 were combined to form the PIP-ETD waveform seen in Figure 4.5 for apomyoglobin $[M+26H]^{+26}$, a protein roughly twice the size and charges of ubiquitin. The precursor notch placement and width will change based on the precursor's m/z. The effectiveness of this PIP-ETD waveform was evaluated in two ways: by parking efficiency and by changes in sequence coverage on standard proteins.

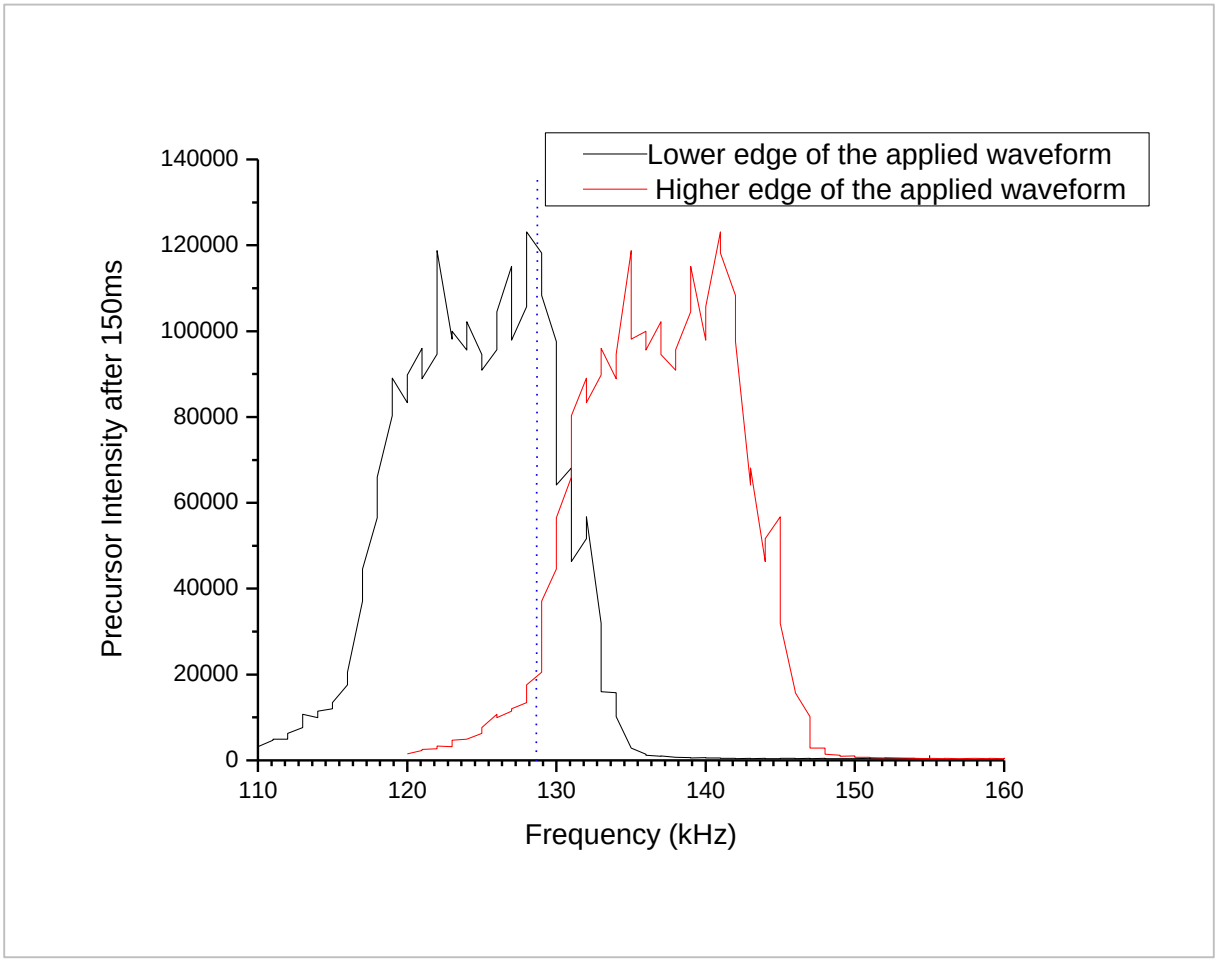

Figure 4.6. To evaluate the necessary precursor notch width in the PIP-ETD waveform, a 14 kHz section of the PIP-ETD waveform is incrementally stepped closer to the ubiquitin $[M+13H]^{13+}$ precursor theoretical secular frequency (128.6 kHz, indicated by dotted blue line). The affects on the ETD reaction rate are shown as plots of the highest and lowest frequencies in the 14 kHz waveform. Similar data was generated for ubiquitin's $[M+12H]^{+12}$, $[M+11H]^{+11}$, $[M+10H]^{+10}$, $[M+9H]^{+9}$, and $[M+8H]^{+8}$.

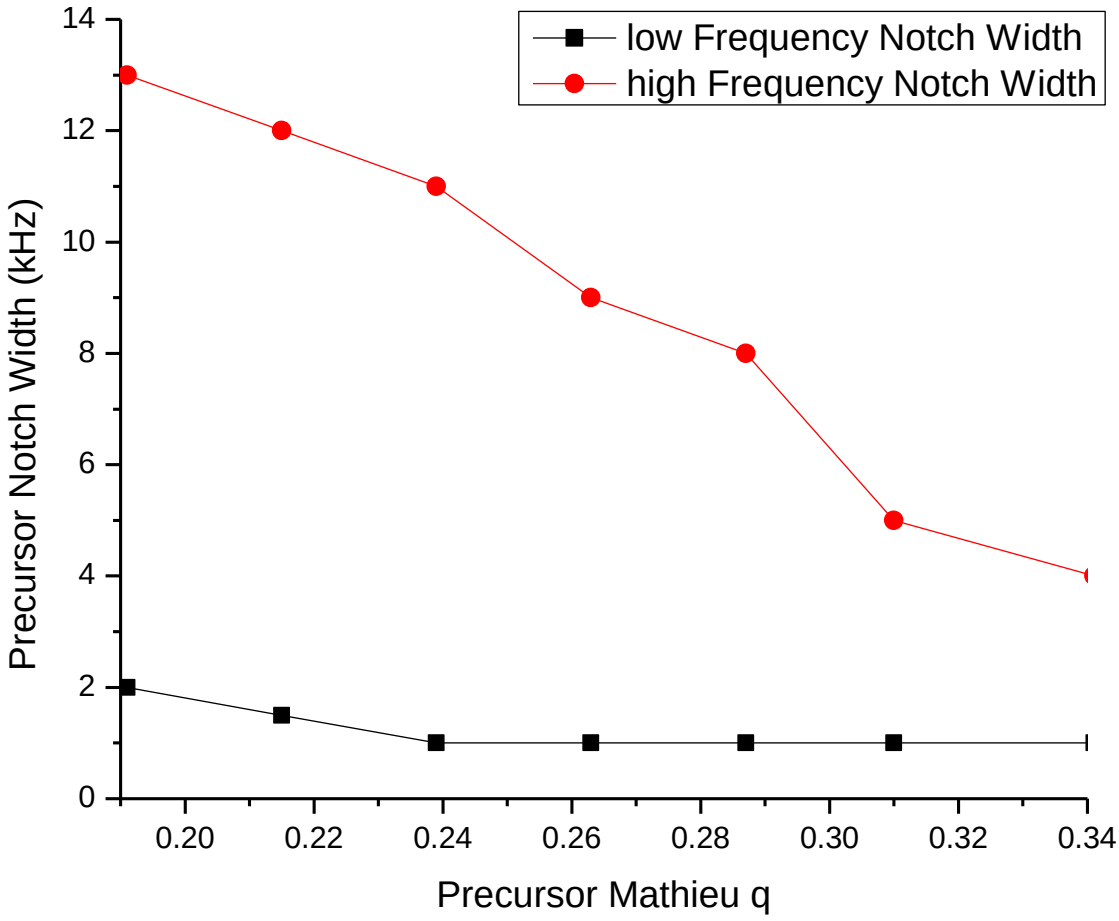

Figure 4.7. From the experiments in 4.4.2, the necessary precursor notch width for frequencies above ("high frequency notch width") and below ("low frequency notch width") the precursor's secular frequency is displayed as function of the precursor's Mathieu q_u.

An ideally efficient PIP-ETD reaction would completely convert the precursor population into product ions, while the product ions remain constant and unreacted. An inherent result of a cation and anion reaction is the neutralization of one charge. As mass spectrometers can only detect

charged species, extensive fragmentation is observed by a loss of product ion signal. This can be seen in Figure 4.8A, where $[M+26H]^{+26}$ of apomyoglobin is reacted by ETD without parallel ion parking. With 20 ms of ETD reaction time, the fragment ions have been so overreacted and charges neutralized, the signal is nearly non-existent. By contrast, Figure 4.8B shows the same reaction using PIP-ETD. Even at extensive reaction times, the fragment ion signal remains steady at its maximum value. This demonstrates the PIP-ETD reaction is very efficient, where the precursor is completely converted into preserved first-generation fragment ions. This evaluation of the waveform was repeated for various charge states of apomyoglobin as the precursor ion. The precursors evaluated are representative of the charge densities typically used for ETD precursors, from roughly 600-1000 m/z. Figure 4.8B-E demonstrates that the PIP-ETD waveform effectively preserves first generation ETD fragments.

To evaluate the utility of the PIP-ETD waveform, PIP-ETD was used to fragment 4 standard proteins: ubiquitin (8.5 kDa), apomyoglobin (17 kDa), histone H1 (20.7 kDa), and Protein G (21.4 kDa). For apomyoglobin $[M+26H]^{+26}$, Figure 4.9A displays the PIP-ETD MS/MS spectrum of 28 ms of ETD. The minute precursor remaining at 653 m/z is favorable, as it means the

precursor is almost entirely converted to products. The most intense peak at 679 m/z in Figure 4.9A is the first charge-reduced precursor, the most abundant first-generation ETD product. The minimal formation of the second charge-reduced precursor at 707 m/z is correlated to minimal second-generation ETD products. The high density of fragment ion signal around the first charge-reduced precursor in Figure 4.9A also indicates the formation of mostly first generation ETD products, but it also makes the spectrum complex and difficult to interpret. Figure 4.9B shows the addition of 25 ms of IIPT reaction after PIP-ETD. All the same fragments are still present, but the m/z signals are now spread throughout the analytical range. This greatly simplified identification of the 220 fragment ions present that generated an 88% sequence coverage. Similarly, 134 fragments of ubiquitin $[M+13H]^{+13}$, 263 fragments of histone H1 $[M+32H]^{+32}$, and 274 fragments of Protein G $[M+26H]^{+26}$ were recovered for 96%, 73%, and 80% sequence coverage respectively. Coverage maps for these proteins are shown in Figure 4.10.

For every ETD reaction, the protein fragments to produce two complementary ions. Identifying complementary pairs is ideal as it greatly increases the confidence of the ion assignments. For larger proteins, it is difficult to observe complementary pairs near the protein termini because

high mass ions have lower signal-to-noise ratios and inefficient transmission through the ion optics. Even if PIP-ETD perfectly prevented higher order ETD reaction products, the m/z signal for high mass ions is split into the ion's various isotopes, which dilutes ion signal into multiple peaks. The weakened signal-to-noise ratio makes detecting those ions harder. Additionally, ion transmission from the LIT to C-trap favors small mass ions due to time-of-flight mass discriminations and more effective collisional cooling. Despite these difficulties, 93% of the fragments identified from ubiquitin were complementary pairs with PIP-ETD, and 78%, 85% and 85% of the fragments were complementary pairs in apomyoglobin, histone H1, and Protein G respectively. These remarkably high identification rates of complementary pairs are primarily a testament of the preservation of first-generation fragments from PIP-ETD.

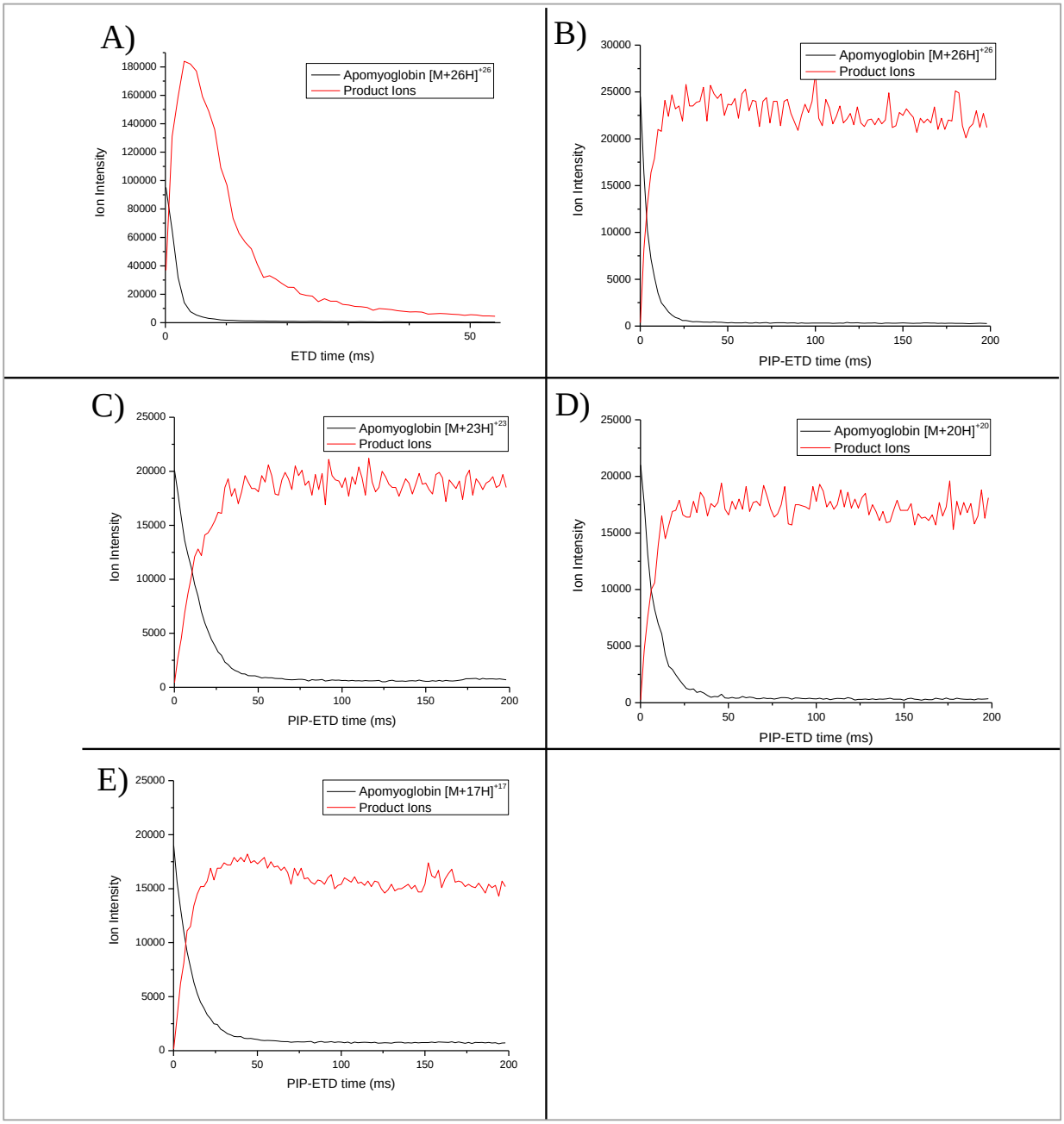

Figure 4.8. Evolution of apomyoglobin precursor and product ions as a function of ETD reaction time. A) The product ion current diminishes quickly with ETD on apomyoglobin $[M+26H]^{+26}$ (653 m/z) without PIP. B) The product ion current is preserved with PIP-ETD on apomyoglobin $[M+26H]^{+26}$ for extended reaction times. C) PIP-ETD with apomyoglobin $[M+23H]^{+23}$ at 738 m/z. D) PIP-ETD with apomyoglobin $[M+20H]^{+20}$ at 848 m/z. E) PIP-ETD with apomyoglobin $[M+17H]^{+17}$ at 942 m/z.

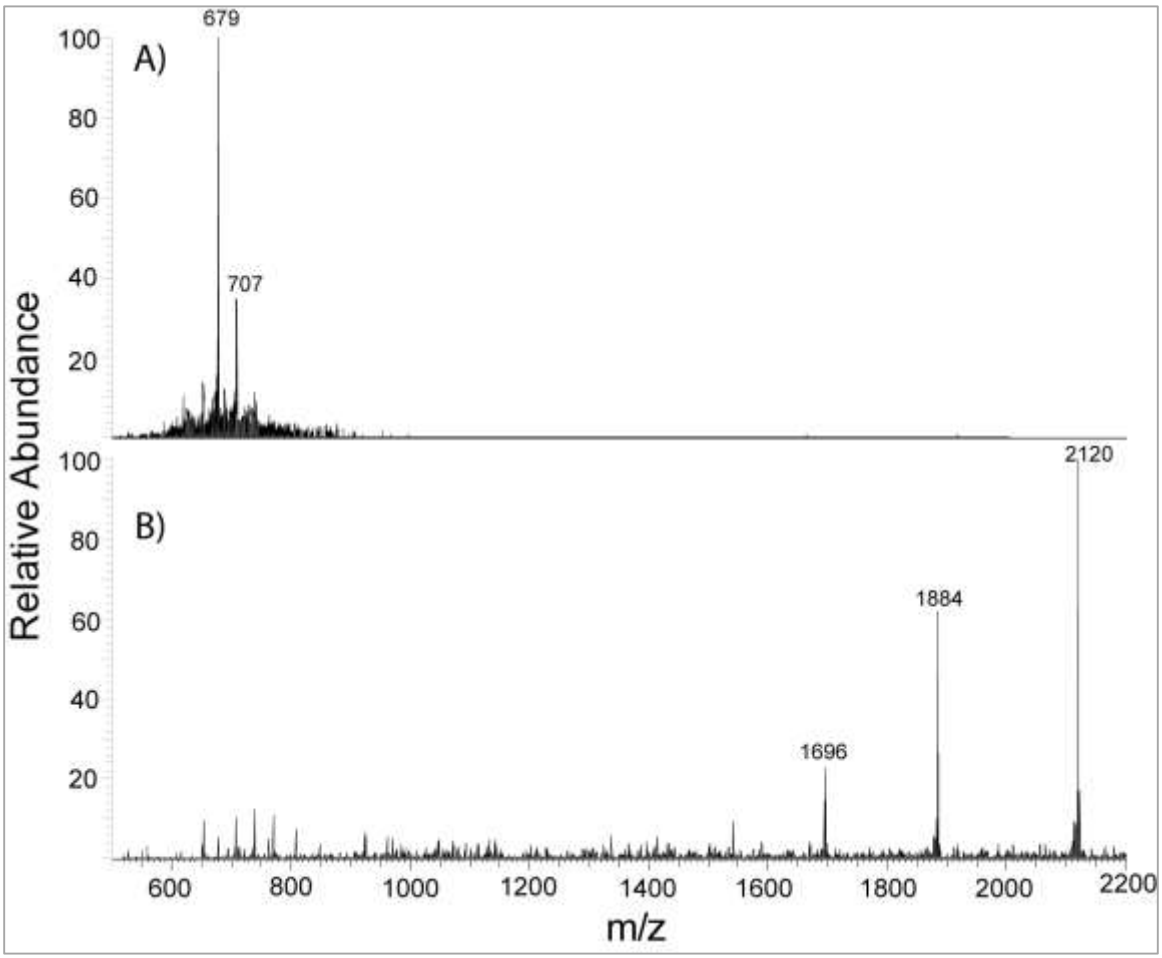

Figure 4.9. A) MS/MS spectrum of 28 ms PIP-ETD on apomyoglobin $[M+26H]^{+26}$. B) MS/MS spectrum of 28 ms PIP-ETD followed by 13 ms IIPT reactions on apomyoglobin $[M+26H]^{+26}$.

Chapter 4

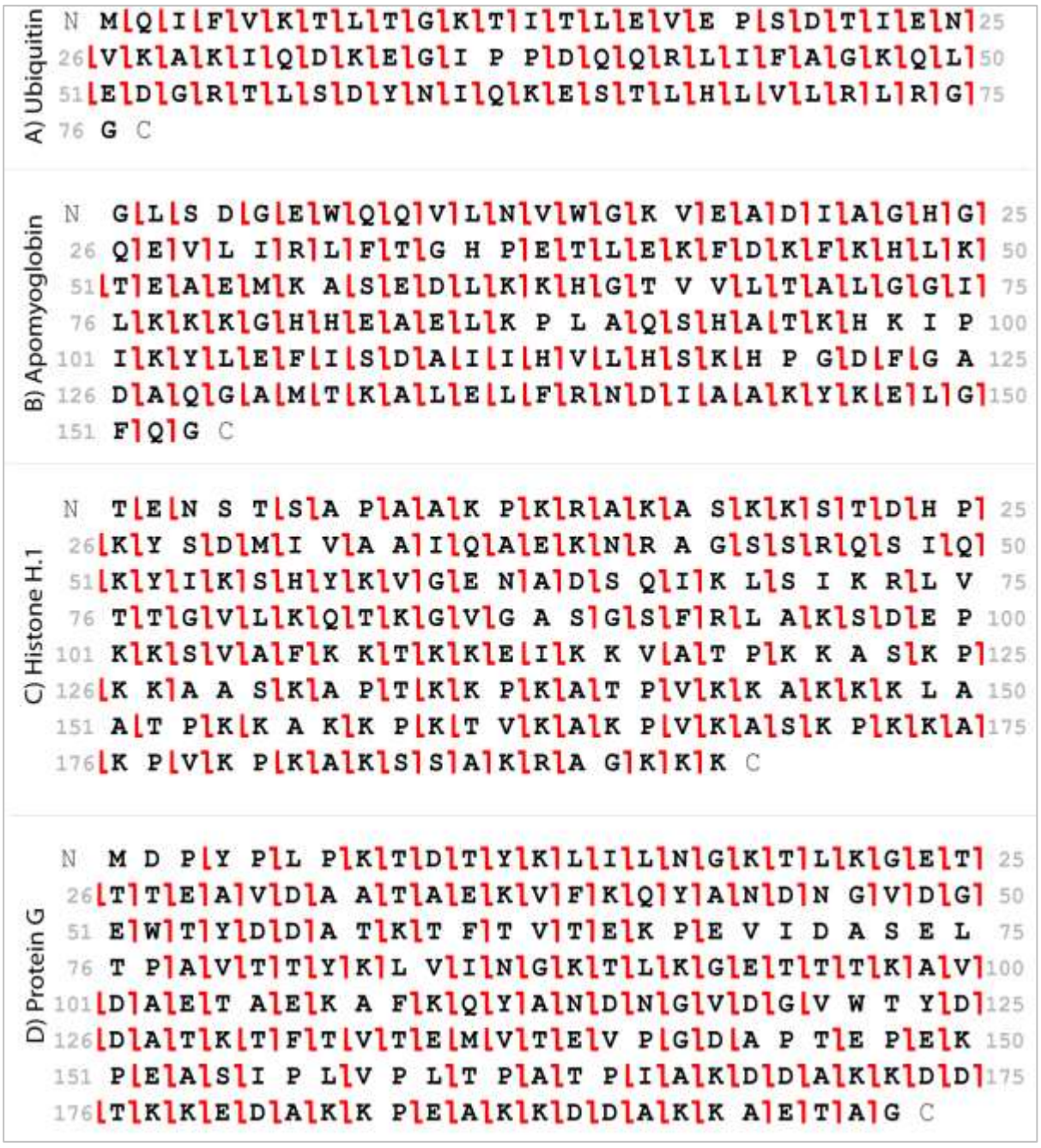

Figure 4.10. Coverage maps of PIP-ETD/IIPT on ubiquitin $[M+13H]^{+13}$ (A), apomyoglobin $[M+26H]^{+26}$ (B), histone H1 $[M+32H]^{+32}$ (C), and Protein G $[M+26H]^{+26}$ (D). Note that ETD does not produce fragments N-terminal to proline.

Chapter 4

4.5 Conclusions

The utility of ETD for intact protein characterization is limited by the production of higher order reaction products. Using PIP-ETD has been shown to help preserve the first generation ETD products in peptides, but applicability to intact proteins has been limited by the lack of an appropriately designed waveform. Calibrations to determine optimal amplitudes and precursor notch widths based on the precursor's Mathieu q_u created a user-friendly waveform, requiring only the precursor m/z to be known for all automated calculations. This work allows for PIP-ETD to be accessible to any researcher to characterize the complete primary structure of unknown, intact proteins ranging from 8kDa to 21 kDa and potentially up to 42 kDa.

Evaluations of the performance of this waveform showed that the precursor ion for a highly charged protein (z=17-26) can be completely and rapidly consumed while product ion signal is preserved for extended periods of time. Evaluations of sequence coverage on 8.5 kDa ubiquitin, 17 kDa apomyoglobin, 20.7 kDa histone H1, and 21.7 kDa Protein G returned 96%, 88%, 73%, and 80% sequence coverage respectively. Furthermore, the high production of complementary ion pairs (93%, 85%, 78%, and 85% of the fragments identified for ubiquitin, apomyoglobin, histone H1, and Protein G

respectively) increases the confidence of assignments and demonstrates PIP-ETD's ability to preserve first generation fragments.

The high incidence of complementary pairs and confidence in preservation of first-generation fragments opens new avenues of interrogation for ETD. Without the confounding variable of higher generation products, it may now be possible to characterize preferred fragmentation sites for ETD. Additionally, examining how external factors, such as reagent excitation, modifications, Mathieu q_u, or amino acid composition, affect the partitioning of first-generation reaction products would give new insight into ETD reactions.

Improvements in instrumentation are necessary to reach the goal of recovering all complementary fragment ion pairs. Many of the small fragment ions lacked their high mass complement, which are inherently harder to identify due to poor ion transmission through the optics and decreased signal-to-noise ratio. Instrumentation has been developed to improve transmission of large ions and with increased resolution capabilities (10). Complete complementary ion recoveries might become feasible if PIP-ETD were enabled on those platforms.

To selectively park all ions except the precursor, the ideal precursor notch would be as narrow as possible. The width is determined by the extent to which the space charged anion cloud distorts the cation's frequencies, as discussed in Chapter 3. If the anion cloud were more diffuse, there would be less of an effect on the precursor cation's frequency. One way to achieve the diffuse anion cloud would be to set it to a lower Mathieu q_u. To do this and still simultaneously stably confine the lower m/z cations, it would be necessary to identify a new ETD reagent with a higher mass.

Chapter 4

4.6 References

1. Zubarev RA, et al. (2000) Electron Capture Dissociation for Structural Characterization of Multiply Charged Protein Cations. Anal Chem 72(3):563–573.
2. Zubarev RA, Haselmann KF, Budnik B, Kjeldsen F, Jensen F (2002) Towards An Understanding of the Mechanism of Electron-Capture Dissociation: A Historical Perspective and Modern Ideas. Eur J Mass Spectrom 8(5):337–349.
3. Chrisman PA, Pitteri SJ, McLuckey SA (2005) Parallel Ion Parking: Improving Conversion of Parents to First-Generation Products in Electron Transfer Dissociation. Anal Chem 77(10):3411–3414.
4. Snyder DT, Peng WP, Cooks RG (2017) Resonance methods in quadrupole ion traps. Chem Phys Lett 668:69–89.
5. Snyder DT, Pulliam CJ, Wiley JS, Duncan J, Cooks RG (2016) Experimental Characterization of Secular Frequency Scanning in Ion Trap Mass Spectrometers. J Am Soc Mass Spectrom 27(7):1243–1255.
6. Williams JD, et al. (1994) Resonance Ejection Ion Trap Mass Spectrometry and Nonlinear Field Contributions: The Effect of Scan Direction on Mass Resolution. Anal Chem 66(5):725–729.
7. McLuckey SA, Reid GE, Wells JM (2002) Ion Parking during Ion/Ion Reactions in Electrodynamic Ion Traps. Anal Chem 74(2):336–346.
8. Holden DD, McGee WM, Brodbelt JS (2016) Integration of Ultraviolet Photodissociation with Proton Transfer Reactions and Ion Parking for Analysis of Intact Proteins. Anal Chem 88(1):1008–1016.
9. Anderson LC, et al. (2016) Analyses of Histone Proteoforms Using Front-end Electron Transfer Dissociation-enabled Orbitrap Instruments. Mol Cell Proteomics 15(3):975–988.

Chapter 4

10. Eliuk S, Makarov A (2015) Evolution of Orbitrap Mass Spectrometry Instrumentation. Annu Rev Anal Chem 8(1):61–80.
11. Ledvina AR, et al. (2010) Activated-Ion Electron Transfer Dissociation Improves the Ability of Electron Transfer Dissociation to Identify Peptides in a Complex Mixture. Anal Chem 82(24):10068–10074.